LAWRENCE
LIVERMORE
NATIONAL
LABORATORY

LLNL-TR-662984

FY14 LLNL OMEGA Experimental Programs

R. F. Heeter, K. B. Fournier, K. Baker, M. Barrios, L. Bernstein, G. Brown, P. Celliers, H. Chen, F. Coppari, D. Fratanduono, M. Gatu Johnson, C. Huntington, A. Jenei, R. Kraus, T. Ma, D. Martinez, D. McNabb, M. Millot, A. Moore, S. Nagel, H. S. Park, P. Patel, F. Perez, Y. Ping, B. Pollock, J. S. Ross, J. R. Rygg, R. Smith, A. Zylstra, G. Collins, O. Landen, A. Wan, W. Hsing

October 21, 2014

Disclaimer

This work performed under the auspices of the U.S. Department of Energy by Lawrence Livermore National Laboratory under Contract DE-AC52-07NA27344.

FY14 LLNL OMEGA Experimental Programs

R.F. Heeter, K.B. Fournier, K. Baker, M.A. Barrios Garcia, l. bernstein, G. Brown, P. Celliers, H. Chen, F. Coppari, D. Fratanduono, M. Gatu Johnson (MIT), C. Huntington, A. Lazicki, R. Kraus, T. Ma, D. Martinez, D. McNabb, M. Millot, A. Moore, S. Nagel, H.-S. Park, P. Patel, F. Pérez, Y. Ping, B. Pollock, J.S. Ross, J.R. Rygg, R. Smith, A. Zylstra (MIT), G. Collins, O. Landen, A. Wan, and W. Hsing

In FY14, LLNL's High-Energy-Density Physics (HED) and Indirect Drive Inertial Confinement Fusion (ICF-ID) programs conducted several campaigns on the OMEGA laser system and on the EP laser system, as well as campaigns that used the OMEGA and EP beams jointly. Overall these LLNL programs led 324 target shots in FY14, with 246 shots using just the OMEGA laser system, 62 shots using just the EP laser system, and 16 Joint shots using Omega and EP together. Approximately 31% of the total number of shots (62 OMEGA shots, 42 EP shots) shots supported the Indirect Drive Inertial Confinement Fusion Campaign (ICF-ID). The remaining 69% (200 OMEGA shots and 36 EP shots, including the 16 Joint shots) were dedicated to experiments for High-Energy-Density Physics (HED). Highlights of the various HED and ICF campaigns are summarized in the following reports.

In addition to these experiments, LLNL Principal Investigators led a variety of Laboratory Basic Science campaigns using OMEGA and EP, including 132 target shots using just OMEGA, 90 shots using just EP, and 6 Joint shots using OMEGA and EP together. The highlights of these are also summarized, following the ICF and HED campaigns.

This work performed under the auspices of the U.S. Department of Energy by Lawrence Livermore National Laboratory under Contract DE-AC52-07NA27344.

Table of Contents

Laboratory Basic Science (LBS) Campaigns 43

Indirect Drive Inertial Confinement Fusion Experiments

1. Thomson Scattering Measurements from Laser-Driven Gold Spheres (PI: J.S. Ross)

with R.F. Heeter and M. Rosen (LLNL), and D. Froula (LLE)

In the FY14 AuSphere and GasCoSphere campaigns, we have performed experiments using high-Z coated spheres illuminated uniformly in direct drive geometry, to investigate atomic physics models and radiative properties of the laser spot plasma relevant to ICF indirect drive ignition hohlraum plasmas. Both bare Au and gas covered Au spheres (shown in Figure 1) were investigated. The laser irradiation of 1e14-1e15 W/cm^2 is similar to the intensities found in NIC hohlraums. The gas covered Au sphere experiments use a gas fill of 1 atm of propane or 1 atm of a 70/30 mix of propane and methane to achieve initial electron densities of 7.5% and 6.0% of the critical density of the 3w drive beams respectively. The plasma temperature and density at various radial positions in the blow-off plasma are characterized using optical Thomson scattering. The probe beam was aligned at various radial locations ranging from 100 to 300 microns from the target surface for Thomson scattering characterization of the low-density plasma blowoff. The laser beams used either a 1ns square laser pulse or a 2-step laser pulse (1 ns square foot, 1 ns square peak) designed to reduce the shock produced by the gasbag window.

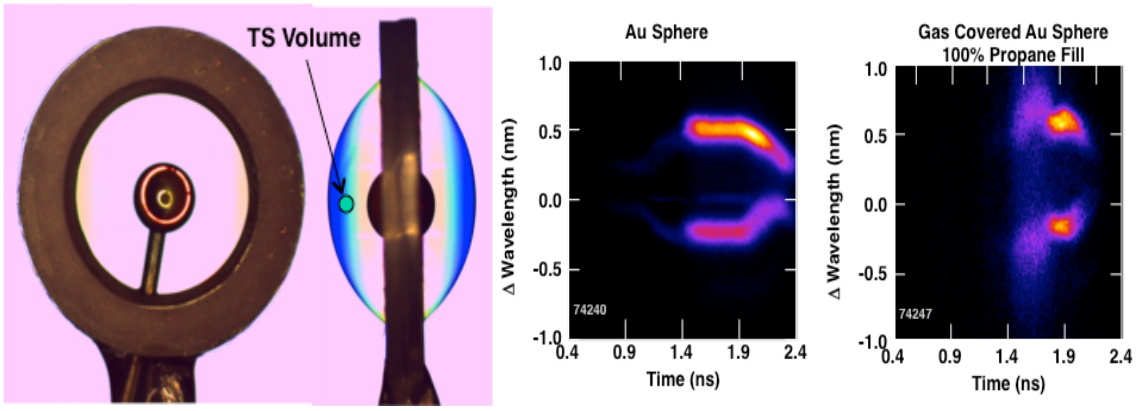

Figure 1: *A 1 mm diameter Au sphere centered in a 2.6 mm diameter gasbag. The gasbag is filled with 1 atm of propane or a mix of methane and propane to achieve different initial electron densities. The location of the Thomson scattering volume is shown.*

The electron temperature and density, the plasma flow velocity, and the average ionization state are measured by fitting the theoretical Thomson scattering form factor to the observed data. Examples of the Thomson scattering data from ion acoustic fluctuations are shown in Figure 1 for both target types. The measured data is then compared to post-shot simulations with different atomic physic and electron transport models. The different models predict different electron temperatures for the experimental conditions, and sample results are shown for the bare Au spheres in Figure 2.

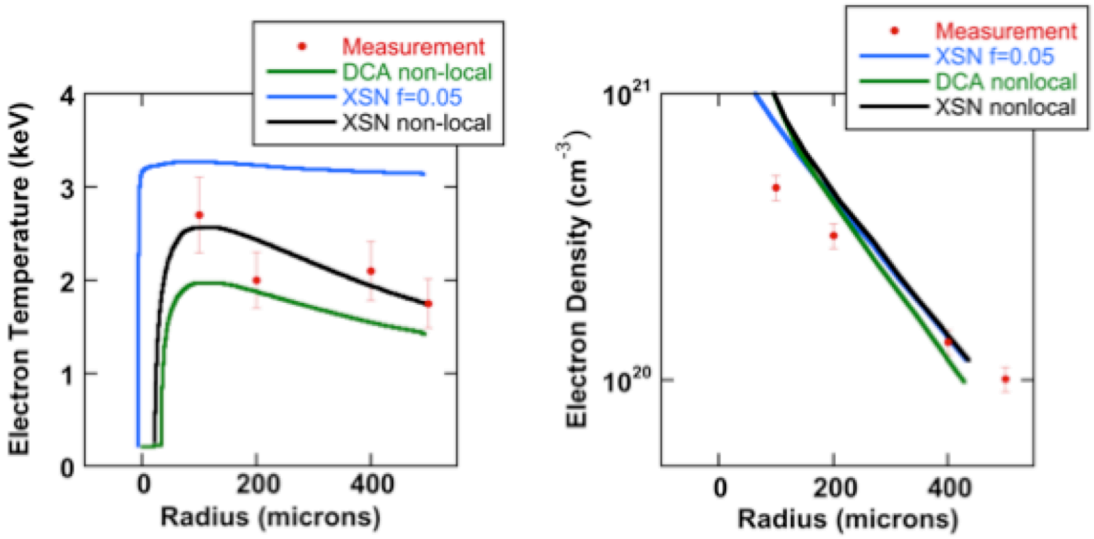

Figure 2: *For bare Au spheres, the measured electron temperature (left) and electron density (right) are compared to post-shot simulations using the DCA nonlocal model (green line), the XSN flux limited model with a flux limiter of 0.05 (blue line), and a non-local heat transport model (black line) for an intensity of* $5x10^{14}$ *W/cm*^{2}.

The simulation with the XSN nonlocal model most closely reproduces the temperatures measured during the experiment. The XSN model with a flux limited transport model using a flux limiter of 0.05, previously used to simulate high-Z hohlraums, predicts an electron temperature significantly higher than measured. A detailed analysis of the gas covered sphere data is currently underway and a comparison of Thomson scattering data, DANTE absolute x-ray flux measurements and X-ray spectroscopy to simulations will be used to further validate the atomic physics models employed in these simulations.

2. Cryogenic Cell Measurements of the Viscosity of Rippled Shocks (PI: P. Celliers)

The ShockViscosity campaigns began as an effort to probe the decay of rippled shocks in NIF ablator materials, as a means of assessing whether the rippled shock response was inviscid or showed evidence of more complicated viscous behavior. As part of this effort attempts were initiated to field a planar cryogenic platform compatible with the viewing axis of the 2D VISAR system (OHRV). The planar cryogenic platform addresses an important surrogacy issue associated with the CAPSEED campaigns. In all prior campaigns, using room temperature targets, a layer of transparent PMMA is used as the surrogate for the fuel layer. The shock-impedance difference between PMMA and ICF ablators is much less than for DT ice or liquid D_2, so any issues associated with the deep release of the ablator into the fuel are not captured accurately in the room temperature PMMA-based platform. For this reason, the cryogenic platform is expected to produce more definitive data sets for the level of ablator non-uniformities transmitted into the fuel. The initial cryogenic shots of the ShockViscosity campaigns were aimed at establishing a baseline data set for the response of various ablators releasing into liquid deuterium. A single baseline data set on GDP was collected during the initial campaign, with other targets leaking due to stress-fracturing of the GDP samples at cryogenic temperatures. Based on this experience, improvements were made to the target design and a second campaign produced several more data sets on HDC and Be ablator samples. The stress-fracturing issue with GDP remains to be solved.

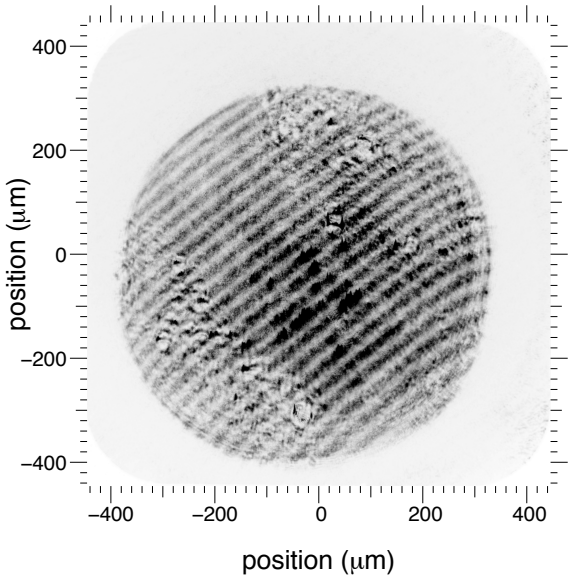

Figure 1*: Interferogram from the first cryogenic test of a GDP ablator releasing into liquid deuterium.*

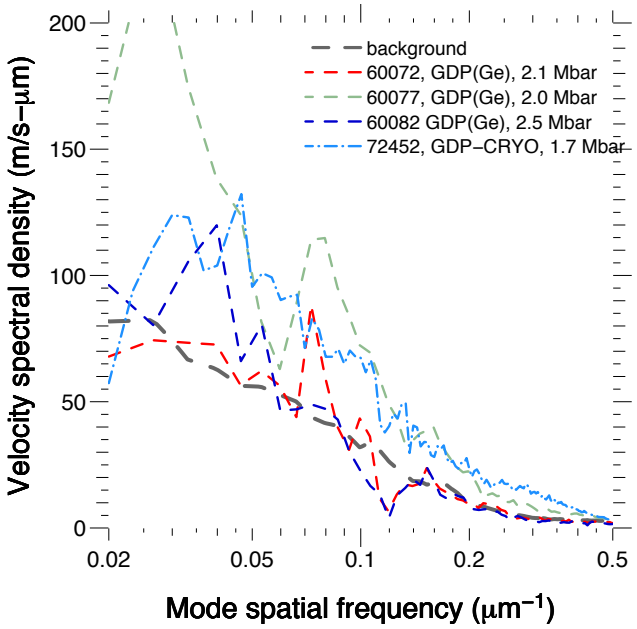

***Figure 2**: Velocity fluctuation spectra measured for GDP on the first cryogenic test of GDP using the OHRV diagnostic, in comparison with data from warm platform tests with PMMA as a surrogate for the fuel. Velocity fluctuation spectra are very similar for the two platforms.*

3. Velocity Fluctuations in Doubly Shocked Glow Discharge Polymer Ablators (PI: P. Celliers)

The CapSeed campaign in FY14 continued our study of glow discharge polymer (GDP), the plastic polymer material used in NIF ablators. The primary goal was to study the response of GDP at the second shock level, by observing the shock front non-uniformities shortly after a second shock, launched behind the initial shock, has overtaken the first. Several shots were devoted to tuning the two-shock drive by adjusting the timing delay between two groups of drive beams. The tuning study was completed and two preliminary data sets were recorded. These initial results did not reveal a level of non-uniformity significantly different from the non-uniformity levels that have been recorded at the first shock level in the GDP material. The current series has laid the foundation for further data collection of GDP using the two-shock drive in a future campaign.

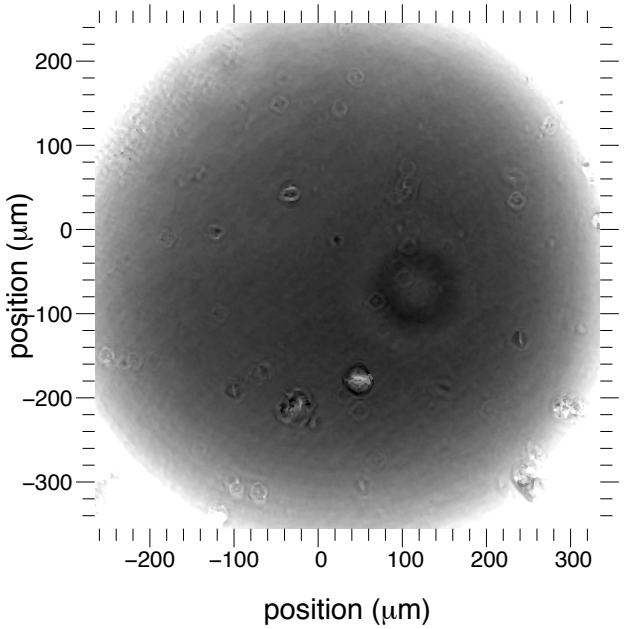

Figure 1*: Gray scale representation of the shock front velocity in a GDP sample double-shocked to ~7 Mbar. The large ripple disturbance originates from a localized defect on the ablation surface; the smaller localized disturbances originate from dust particles trapped at the GDP-PMMA interface during target assembly.*

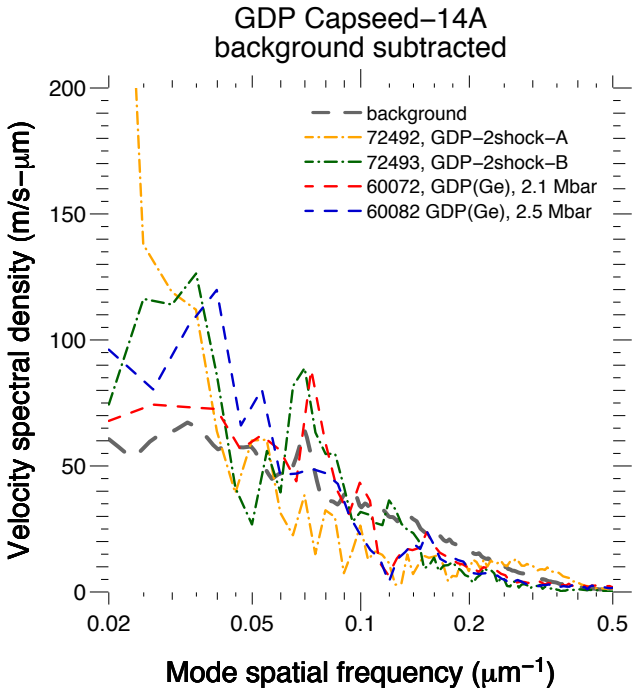

***Figure 2**: Velocity fluctuation spectra measured for GDP on two double-shock GDP experiments compared with earlier single shock tests. Spectra are background-subtracted. The background level is shown for comparison.*

4. Shock Release Isentrope Measurements of ICF-Relevant Materials (PI: D. Fratanduono)

To address concerns regarding uncertainties in the release isentropes of ICF ablator materials into low-density gas, experiments were performed to measure the release of GDP and CH into methane gas at gas densities comparable to an ICF capsule, to examine the momentum transfer in this low-density kinetic regime. The experiment measured the shock velocity in the GDP prior to shock breakout, and the shock transit time through a known methane gas density (0.25-1.0 atm). We then utilized a momentum transfer technique to extract P-Up data (the release isentrope). These experiments suffered unexpectedly from non-reproducible effects, which made it difficult to distill conclusions. On average, the shock velocity in the methane gas was anomalously low, suggesting that the equation of state model may be over predicting the release state. Since the results were not consistently reproducible, future experiments will be required to examine this region of phase space in detail

5. Platform Development for Measuring Charged-Particle Stopping in Warm Dense Plasmas (PI: A. Zylstra, LLNL/MIT Collaboration)

The TransportEP-14A campaign conducted shots to continue development of a stopping-power measurement platform using the short-pulse lasers on Omega-EP. In this experiment, the sidelighter beam was used for proton isochoric heating of a warm dense matter sample, while the backlighter beam drove a planar foil, generating protons via target-normal sheath acceleration (TNSA) to probe the sample. For the backlighter-driven proton source, the uniformity of the proton beam was studied using source-only shots with a lower-energy drive (40J/1ps) and smooth wafer targets of CVD and Si, in comparison to standard Au. The proton beam images are shown in Figure 1(a) to (c). While the uniformity is improved over previous higher-intensity shots, modulations in the proton beam remain. The proton isochoric heating configuration sends a TNSA proton beam through a CH slab (200x200x50um), which is heated by proton energy deposition and characterized by X-ray backlighting. The backlighter was a uranium area backlighter, with data taken from 0.5ns before the slab is heated until 1.5ns after, as shown in Figure 1(d). Preliminary data analysis suggests non-thermal expansion potentially driven by electromagnetic fields.

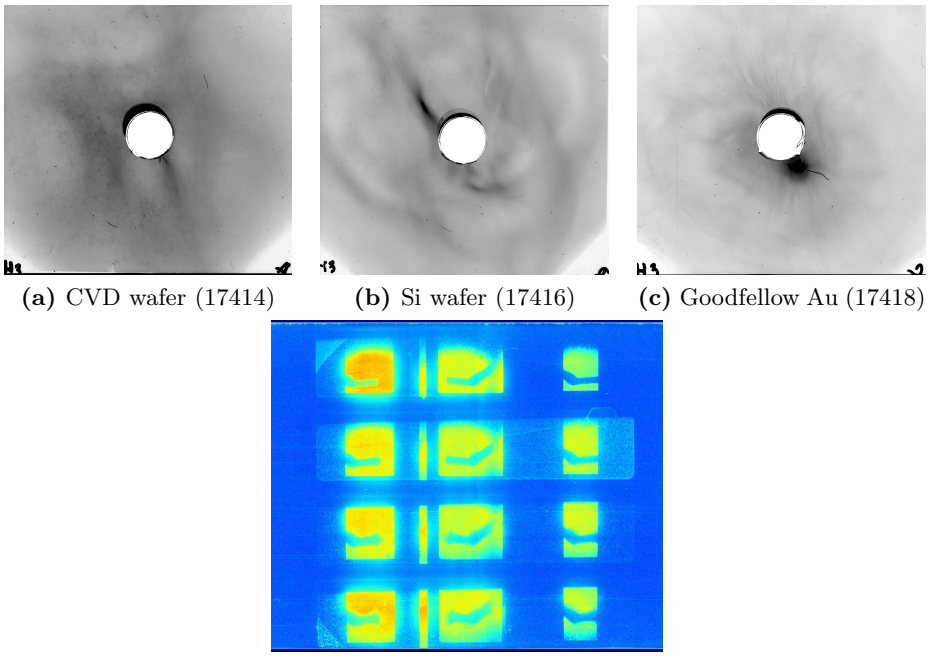

(a) CVD wafer (17414) **(b)** Si wafer (17416) **(c)** Goodfellow Au (17418)

(d) X-ray radiographs of heated slab

Figure 1: *Proton source spatial distribution images (a-c) for various foil targets, and (d) x-ray radiography of proton-isochoric-heated slabs.*

6. Measurements of the Opacity of Silicon in ICF Ablator Conditions (PI: R.F. Heeter)

with G.V. Brown, C. Mauche and B. Wilson

Continuing earlier ablator opacity measurements, improved experiments were performed to measure the transmission opacity of hot silicon at $T \approx 70$eV, $\rho \approx 0.2$ g/cc at Omega-EP. At these temperatures and densities from 0.2 to 20 g/cm^3, there is a strong sensitivity of the Atwood number in Si-doped capsules to the Si opacity. The FY14 experiment used a Be-tamped Si foil sample, heated by 250J, 250ps impulses from 2 of the long pulse beams. The sample plasma was characterized with dual-axis, simultaneous backlighting, both face-on and edge-on, using the 2 short pulse beams in 10 ps mode. The backlighters were timed 200 ps after the peak of the heating impulse, as verified with the ultra-fast X-ray streak camera. The edge-on radiograph measures density via the sample expansion from a known initial thickness (2.1 μm); the face-on measurement delivers Si ionization balance and transmission opacity data via absorption spectroscopy across the X-ray band from 1600 eV to 3000 eV. To probe the sample at higher density than previously, the edge-on radiography was improved by using a smaller backlighter and samples with improved planarity. The new technique delivered ~10 μm resolution, verified by radiographing a cold 10 μm Cu wire and also by discriminating the continuum absorption of the heated Si from the weaker absorption of the underlying Be substrate. The target density of 0.2 g/cm^3 was achieved by probing the Si plasma 200ps after the peak of the heating pulse, when the silicon had expanded to 20 μm. As illustrated in Figure 1, the Si measurements show absorption features from at least 5 of the L-shell charge states of Si, plus time-integrated self-emission from earlier in the heating pulse. This high quality data set will be analyzed and compared with the opacity models used for the NIF capsules.

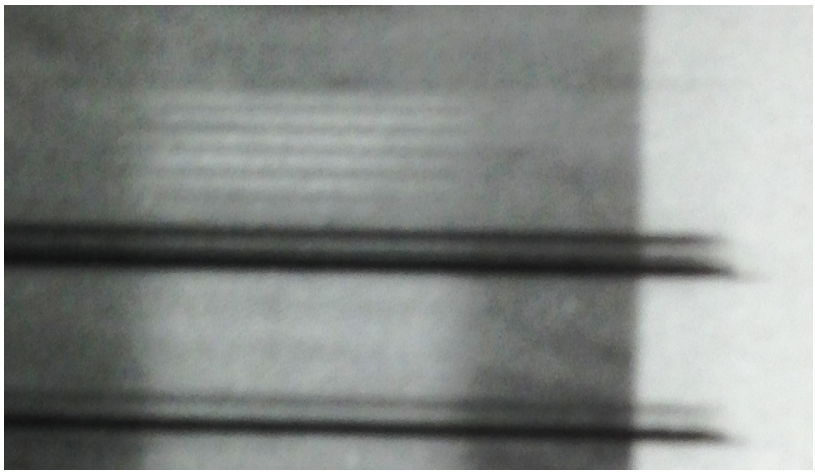

Figure 1: *Space-resolved absorption spectrum obtained on Omega-EP, using face-on broadband spectroscopy from a Zn bremsstrahlung continuum backlighter. Photon energy increases from top to bottom; emission is dark and absorption is light. Multiple time-resolved absorption and time-integrated emission features of hot silicon are detected with excellent signal-to-noise.*

7. Hohlraum Magnetization Using Laser-Driven Currents (PI: B. Pollock)

with J. Moody, J.S. Ross and D. Turnbull

In FY14 the HohlFaradayRot campaigns on Omega EP, and the BFieldHohl campaign on Omega launched an investigation of the feasibility of self-magnetizing hohlraum targets for ICF applications. The first campaign in this new experimental effort employed a target consisting of a half-loop formed by folding a thin gold sheet around a 500 um diameter fused Si rod. Figure 1 illustrates how the EP long pulse beams shine through holes in one of two parallel plates on the open side of the loop, producing a plasma at the surface of the second plate. Hot electrons formed by this process collect around the holes in the first plate, essentially charging up a parallel plate capacitor. The half-loop connects the plates, allowing current to flow and produce a magnetic field on the loop axis. The EP 4w probe capability was employed to directly measure the magnetic field inside the loop via Faraday rotation along the hohlraum axis. Fields up to 4.6 T were measured at the time of the probe beam. A new B-dot probe was also developed for this campaign, and acquired signal on all shots. Combining the B-dot probe data with a second set of Faraday rotation measurements from a second piece of fused Si outside of the loop, the peak field produced is inferred to be ~40 T. In the second HohlFaradayRot shot day, the short-pulse backlighter beam was used to drive a proton source for proton deflectometry measurements of the fringing magnetic fields around the target. This campaign allowed additional parameter scans and extended the previous data set.

The BFieldHohl campaign transitioned the experiment to Omega, taking advantage of the 60 beams available and increasing the target diameter from a 0.5 mm half-loop to a 2.0 mm, nearly complete loop. Similar to the EP experiment, the magnetic field was driven by using 14 beams to illuminate parallel plates. Another 8 beams were directed into the loop to heat the quasi-hohlraum, and the fringing magnetic field outside of the target was diagnosed with proton deflectometry from a D^3He capsule source. The analysis of this recent experiment is ongoing and will inform the FY15 continuation of this effort.

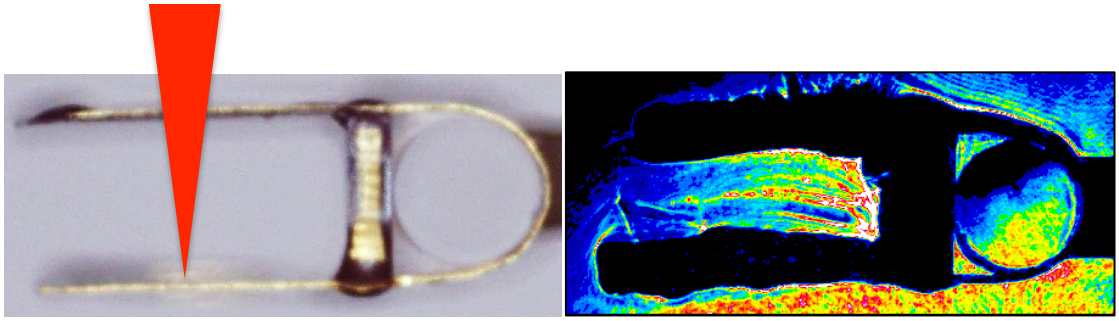

Figure 1: *(Left) Geometry for hohlraum self-magnetization on Omega-EP, with beampath shown schematically in red. (Right) Sample of 4w probe data used to infer Faraday rotation.*

High-Energy-Density Experiments

I. Material Equation of State Using Diffraction Techniques

A. Kinetics of Melting in Iron (PI: R. Kraus)

with F. Coppari, D. Fratanduono, A. Lazicki, D. Swift, J. Eggert and G. Collins

The iron melting curve at multi-Mbar pressures is critical to understanding the Earth's thermal state and also how its magnetosphere formed and evolves. Dynamic experiments can probe the melting transition at pressures near the inner-core boundary of the Earth (~330 GPa). Nguyen and Holmes (2004) previously studied the melting transition with a gas gun,[1] using sound velocity measurements, but concerns about the results were raised due to the possible kinetics of melting.

This issue was addressed using in situ x-ray diffraction at the Omega laser facility to directly probe the onset and completion of melting along the principal Hugoniot. Polycrystalline diffraction from the high-pressure hexagonal close packed (hcp) phase of iron was monitored. As the iron was shocked to higher-pressure states along the melt curve, we observed an intensity decrease for the solid diffraction lines together with an increase in the diffuse scattering signal. Attributing this to liquid scattering (Figure 1), we have shown that both incipient and complete melting occurred at the same stress states on the laser timescale (ns) as the gas gun timescale (100's of ns), so the kinetics of melting are negligible for these timescales and longer. The data also show that iron stays in the hcp phase along the melt curve until nearly 270 GPa, clarifying an issue that has been debated theoretically.

References:

1. Nguyen, J. and Holmes, N. C., "Melting of iron at the physical conditions of the Earth's core", *Nature* **427**, 339 (2004).

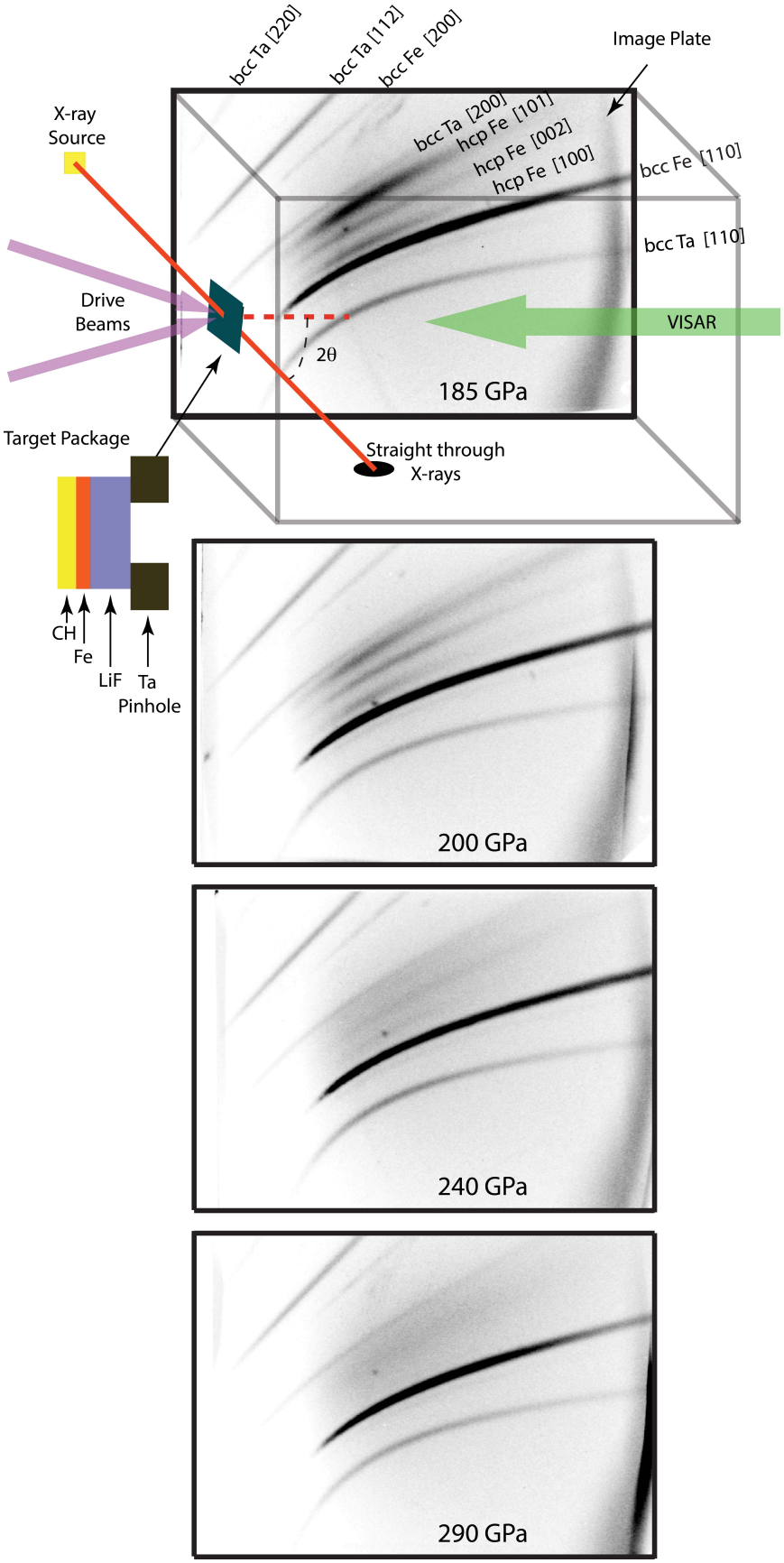

Figure 1: *(Top) Geometry for in-situ x-ray diffraction on Omega laser facility. Also shown are image plate data for shock induced melting of iron, with a decrease of intensity in the solid diffraction signal and increase in the diffuse background as melting occurs at higher shock pressures.*

B. Kinetics of Melting in Tin (PI: R. Kraus)

with F. Coppari, D. Fratanduono, A. Lazicki, D. Swift, J. Eggert and G. Collins

In this campaign, we used the PXRDIP diagnostic to obtain in-situ x-ray diffraction at the Omega laser facility. Tin has a complicated high-pressure phase diagram, and the melting curve of tin has come under recent debate. Prior measurements of the melting temperature up to 1 Mbar show a dramatic increase in the slope of the melting curve as the solid phase transitions from a body-centered orthorhombic (bco) to body-centered cubic (bcc) structure.[1] Phase transitions in tin are also thought to be sluggish in comparison with other metals.[2] Our campaign's goal was to probe directly the onset and completion of melting along the principal Hugoniot of tin, and compare the data with different timescale experiments to learn about the kinetics of melting. For shock pressures below 50 GPa, the data show strong textured diffraction from the high-pressure phase of tin, whereas above 60 GPa the data show a strong diffuse scattering signal from liquid tin. These data bracket the melting transition along the principal Hugoniot, in agreement with significantly longer timescale gas gun experiments.

1. Briggs, R. *et al.,* "Melting of Sn to 1 Mbar", *Journal of Physics: Conference Series* **377**, 012035 (2012).
2. Luo, S. N., Ahrens, T. J., "Shock-induced superheating and melting curves of geophysically important minerals", *Physics of the Earth and Planetary Interiors* **143-144**, 369–386 (2004). doi:10.1016/j.pepi.2003.04.001.

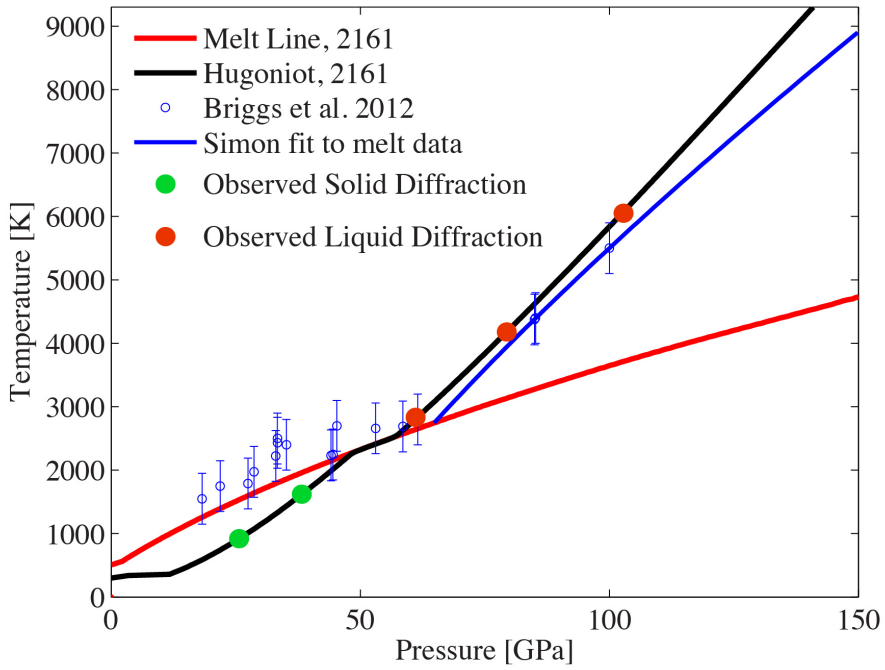

Figure 1: *Pressure-temperature phase diagram for tin, showing the melting curve data from Briggs et al. 2012. Plotted along the Hugoniot of the 2161 SESAME equation of state are the pressure states where we observe solid diffraction (green) and liquid diffraction (red).*

C. Shock-Resolidification Kinetics of Tin and Iron (PI: R. Kraus)

with F. Coppari, D. Fratanduono, A. Lazicki, D. Swift, J. Eggert and G. Collins

The Diffraction-EP campaign extended the earlier Omega experiments on melting kinetics of iron and tin by using Omega-EP to probe the time scale for re-solidification of both materials. Having previously shown that tin and iron can be shock melted on the timescale of a laser-shock experiment, and that melting occurred at the same pressures as in gas gun experiments (to within the error bars of our measurements), these EP experiments sought to quasi-isentropically compress tin and iron from shock-melted states back across the melt curve into the solid phase.

In the tin experiments, we generated an initial shock that was consistently at ~65 GPa (into the liquid phase), and then generated a second shock that brought the tin to a peak pressure of ~160 GPa. The first shock set the initial thermodynamic state of the tin in the liquid phase, and the second shock quasi-isentropically compressed the tin into the solid stability field. After some tuning we accurately timed the second shock and the backlighter, and Figure 1 shows the observed strong polycrystalline diffraction peak from re-solidified tin. These results are the first unambiguous observation of pressure-driven solidification in a metal. They show great promise that we can probe the kinetics of solidification using laser-shock platforms, and that in-situ x-ray diffraction provides an important tool in diagnosing the re-solidification process.

In the iron experiments, we successfully observed strong diffraction from high-pressure hexagonal close-packed (hcp) iron, diffuse liquid scattering, and a very preliminary signature of re-solidification. However, the initial thermal state in the liquid could not be accurately confirmed due to issue with this initial experiment.

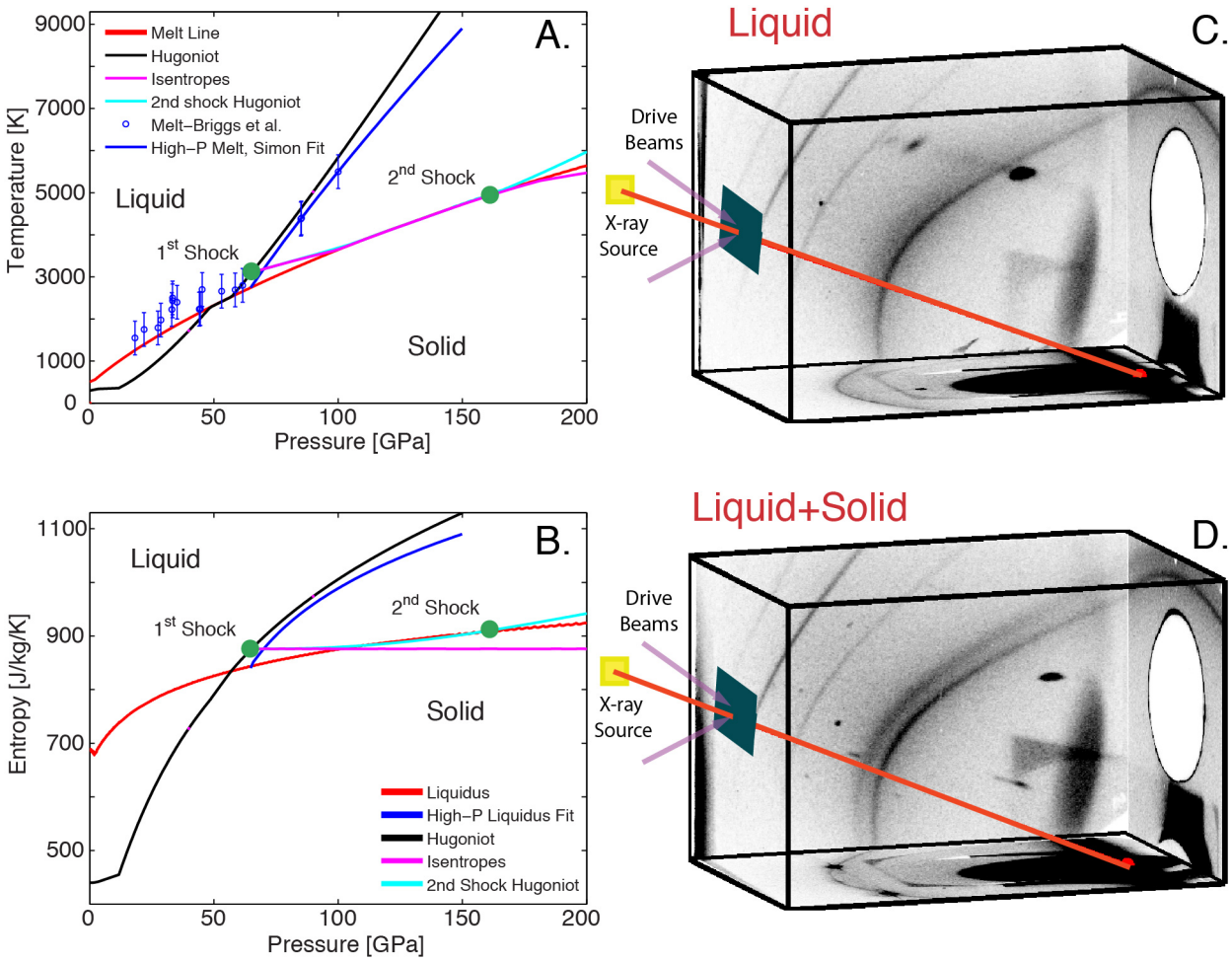

Figure 1: *A. Pressure-temperature phase diagram for tin from the SESAME 2161 equation of state. Static melting curve measurements (blue points) are from Briggs et al. (2012) B. Pressure-entropy phase diagram for tin from SESAME 2161. C & D. Image plates from a double shock experiment on Sn (first shock to 65 GPa, second shock to 160 GPa). The second shock in C is timed so that the x-rays principally interact with unshocked and single shocked material. The second shock in D is timed so that a larger volume of material reaches a second shock state of 160 GPa. Note the strong polycrystalline diffraction line observed in (D) that does not exist in (C).*

D. Improving the Omega High-Pressure Tantalum Diffraction Platform (PI: F. Coppari)

with J. Eggert, R. Smith, D. Fratanduono, A. Lazicki, and R. Rygg

This campaign improved the tantalum diffraction platform using the PXRDIP diagnostic at Omega by resolving issues related to the high background signal observed in high pressure shots, and sought to understand texture evolution when the sample material is ramp-compressed to high pressure states. Mitigation schemes were tested that decreased the background signal and improved the platform overall. In particular, a tungsten wire, placed in a specific location of the diagnostic, provided a geometric trace of the background source. Although most of the background is due to the ablation-generated plasma, some background also comes from the fluorescence of the image plates when hit by the direct x-ray beam. To mitigate this source of background, a fluorescence shield was implemented using a Ta skewed cylinder placed around the region where the direct x-rays hit the image plate (Figure 1). This mitigation scheme has also been adopted in the diffraction platform on NIF with the TARDIS diagnostic.

The second goal of the campaign was to start looking at the texture formation and evolution in ramp-compressed materials and in particular Ta. The shots compared diffraction from Ta samples with three different initial textures: commercial foils, coatings and pressed powder. Preliminary characterization of the initial texture by laboratory x-ray diffraction and pole-figure analysis indicated that foils and coatings are characterized by a strong fiber texture, while the pressed-powder samples are randomly oriented, so that the corresponding diffraction signal is an untextured diffraction ring. The data show that when laser-driven ramp compression is used to achieve high-pressure states in these three materials, the initial texture is preserved at high pressure and also across a phase transition. The initially untextured powder remained untextured, while samples with initial fiber texture showed a highly textured diffraction signal, which persisted even above a solid-solid phase transition. This suggests that some sort of memory mechanism may take place that certainly deserves further investigation in future campaigns.

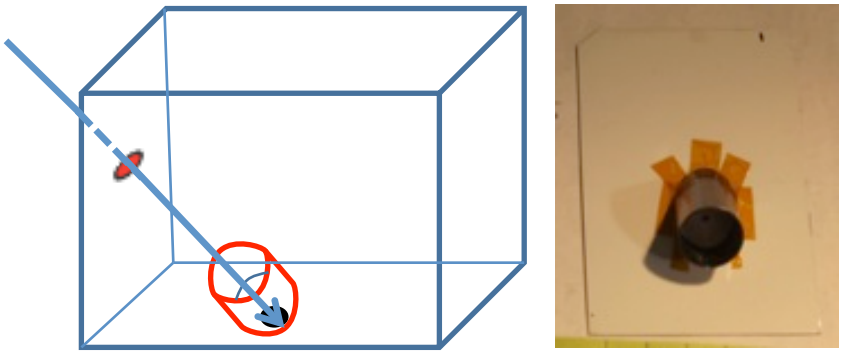

Figure 1: *Fluorescence shield used at Omega to block x-rays generated by the fluorescence of the bottom image plate hit by the direct x-ray beam. On the left is a sketch of the position of the shield within the PXRDIP diagnostic and on the right a picture of the shield on the image plate.*

E. Development of Higher-Energy Backlighters for X-Ray Diffraction (PI: R. Smith)

The goal of these shots was to develop and optimize Zr He-alpha (16.3 keV) and Ge He-alpha (10.3 keV) x-ray sources for future x-ray diffraction experiments on Omega, Omega-EP and NIF. The standard x-ray source for diffraction on Omega, using the PXRDIP diagnostic, is the Cu He-alpha quasi-monochromatic line emission at 8.3 keV. In those experiments[1] the main noise contributor at high sample pressure is from thermal x-rays generated in the sample drive plasma. In order to increase the signal-to-noise of x-ray diffraction experiments, higher energy sources are needed which are spectrally decoupled from the drive plasma emission spectrum to enable more effective noise filtering.

The targets for these experiments consisted of a free standing 2x2mm, 10μm-thick Zr foil or a 6 μm Ge layer coated on both sides of a 200 μm pyrolytic graphite substrate. The spectrally resolved emission for a range of laser irradiance conditions was recorded with the XRS Rowland spectrometer and the NRL Dual Crystal Spectrometer (DCS) which covers the x-ray bands from 10.4-45 keV and 20-120 keV. To optimize the output from Zr He-alpha, up to 20 Omega beams were employed in a double-sided illumination geometry. Pre-pulse and main-pulse laser irradiance conditions on the Zr foil were systematically varied, and the resulting He-alpha production measured. The laser power as a function of time was varied shot-to-shot as illustrated in Figure 1. The resultant PSL (photo-spectral luminescence) counts on the XRS spectrometer image plates from the He-alpha line per kJ of main pulse laser energy are shown in Figure 2 as a function of the main pulse energy and intensity. The peak 16.3 keV He-alpha production occurs at an intensity of ~8×10^{15} W/cm^2. A similar experimental approach and analysis for Ge suggests that the He-alpha optimization occurs at a laser intensity of 1×10^{15} W/cm^2.

References:

1. J.R. Rygg, J.H. Eggert, A.E. Lazicki, F. Coppari, J.A. Hawreliak, D.G. Hicks, R.F. Smith, C.M. Sorce, T.M. Uphaus, B. Yaakobi, and G.W. Collins, *Rev. Sci. Instrum.* **83**, 113904 (2012).

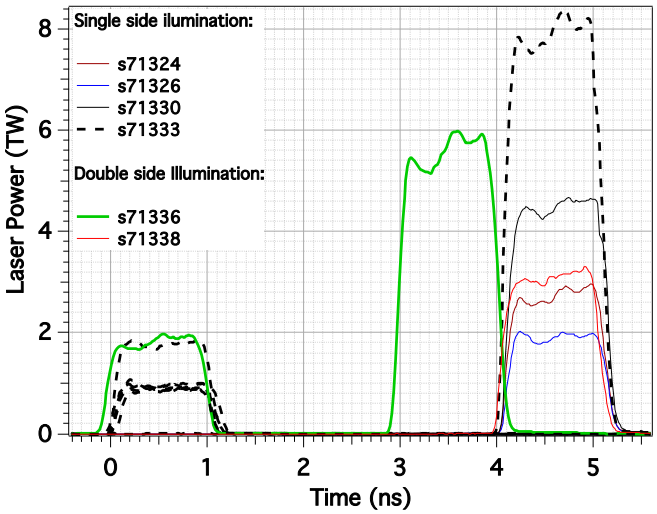

Figure 1: *Laser Power versus time for Zr He-alpha backlighter development campaign.*

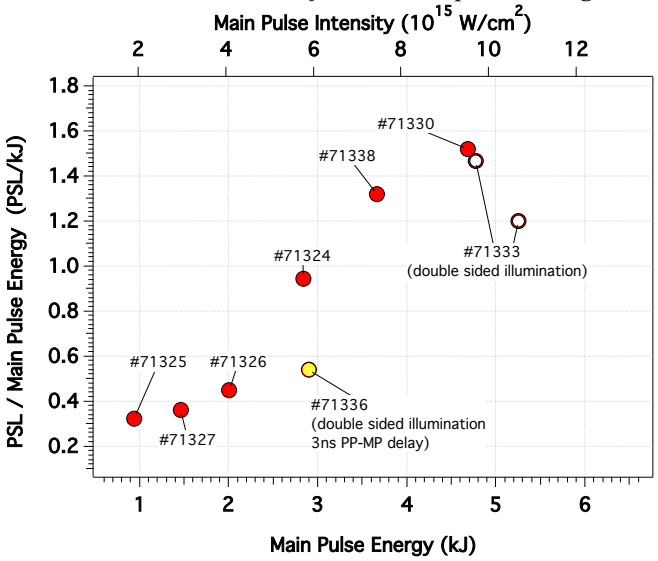

Figure 2: *PSL (photo-spectral luminescence) counts on the XRS spectrometer image plates from the 16.3 keV Zr He-alpha line per kJ of main pulse laser energy is shown as a function of the main pulse energy and intensity.*

II. Material Equation of State Using Other Techniques

A. Measurements of the Lithium Hydride Equation of State (PI: A. Jenei)

with J. Hawreliak, R. London, D. Fratanduono, and G. Collins

The LiH equation of state measurements started in FY13 were completed in FY14, providing data to constrain the shock Hugoniot equation of state (EOS) of LiH between 0-10 Mbar. Two different techniques were employed to determine the shock Hugoniot. The first method used velocimetry data from the VISAR diagnostic to infer the velocities of reflecting shocks in a target with layers of single crystal quartz and single-crystal LiH, and pyrometry data from the SOP diagnostic to determine temperatures. Quartz was used as the EOS reference standard for determining both the velocities and temperatures in LiH. Figure 1(a) shows an example of the raw data from this configuration, which succeeded in measuring the Hugoniot up to nearly 12 Mbar.

In the second approach, a framing camera radiographed the shock front and pusher/sample interface positions as a function of time in a shock-compressed sample backlit using a chlorine-doped plastic (2.8 keV) area backlighter. The motion of these fronts can provide absolute data on the shock and particle velocities. Although the pulse length was insufficient to generate a steady shock for long enough to make an accurate EOS measurement, this experiment demonstrated successful imaging of the interfaces, as shown in Figure 1(b). The information gathered about contrast and resolution provided valuable feedback for future experiment designs.

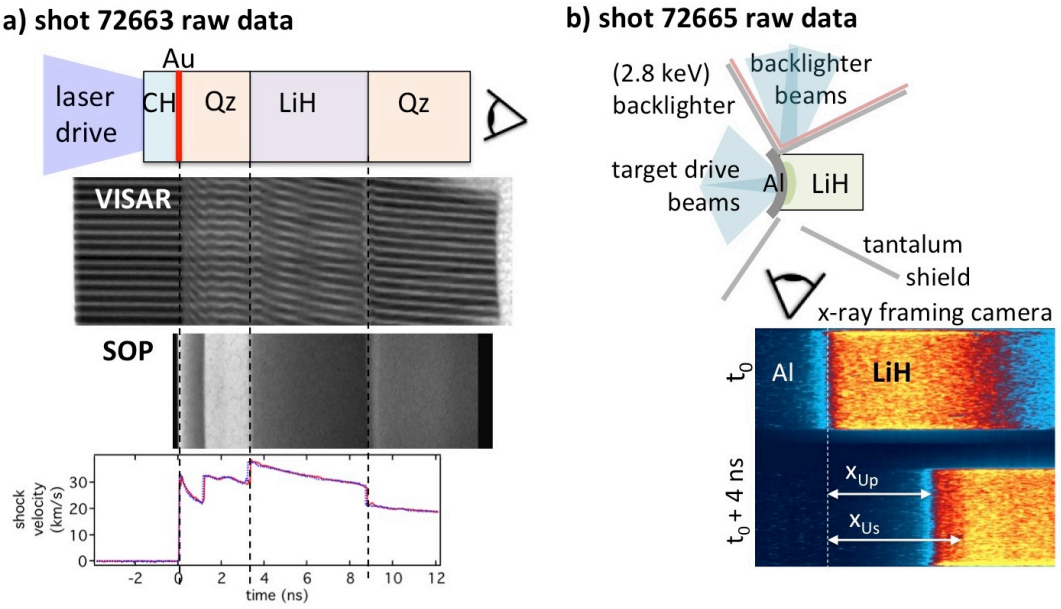

Figure 1: *LiH equation of state measurements using (a) shock Hugoniot configuration and sample data using quartz as a reference standard; (b) radiographic configuration and sample data for absolute EOS measurements.*

B. Equation of State Measurements on Single Crystal Diamond (PI: D. Fratanduono)

NIF diffraction equation-of-state experiments utilize single-crystal diamond in the target design in order to ramp compress the sample to high pressure and minimize the diffraction signal from the diamond. These experiments require an accurate stress-density response of single-crystal diamond. Previous OMEGA (Bradley 2008) and NIF experiments (Smith 2014) measured the stress-density response of CVD (polycrystalline) diamond, but there has been concern that the stress-density response of single crystal diamond (<100> and <110>) could be different from the CVD measurements. To address this, experiments were performed at OMEGA to measure the response of single-crystal diamond in the <100> and <110> orientations, with a key result shown in Figure 1. The stress-density response of single crystal diamond is in excellent agreement with the stress-density response of CVD (polycrystalline) diamond, but results indicate that the 'pullback' features observed in NIF experiments are significantly reduced in the <110> orientation when compared to <100>. Radiation-hydrodynamics simulations have demonstrated better predictive capability for the <110> orientation versus <100>, but the EOS at high pressure needs to be improved. Future "A vs. B comparison" experiments of the EOS of diamond <110> vs <100> will greatly assist in our development of a diamond strength model, and will further probe the stress-density response up to 10 Mbar.

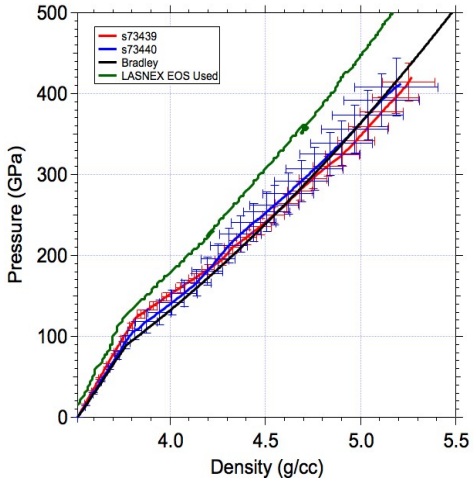

Figure 1: *Newly measured pressure-density equation of state data for single-crystalline diamond (red, blue), compared with prior data on polycrystalline diamond (black) and a reference EOS model (green).*

C. Extended X-Ray Absorption Fine Structure Measurements of Ramp Compressed Ta up to 200 GPa (PI: Y. Ping)

with F. Coppari, B. Yaakobi, J. H. Eggert and G. W. Collins

Based on successful improvements of the extended X-ray absorption fine structure (EXAFS) platform in FY13,[1] high-quality EXAFS data of compressed Ta up to 200 GPa were obtained in FY14. The spectra at three pressures are shown in Figure 1. The data at ambient conditions, and at 65 GPa are consistent with Ta in the bcc phase, whereas the data at 200GPa cannot be fit with the bcc phase, indicating that Ta undergoes a phase transition above 1Mbar. Subsequent shots reached 350GPa, however the quality of this EXAFS data was not as good as previous data. Two reasons have been identified. First, the target alignment fiducial was not as accurate as before, reducing the number of observable channels from 5 to 2, significantly degrading the S/N ratio. Second, the backlighter brightness was ~40% less than on prior shots for reasons under investigation but not yet understood. Both findings provide important guidance for upcoming FY15 shots.

1. Y. Ping, D. G. Hicks, B. Yaakobi, F. Coppari, J. Eggert and G. W. Collins, *Rev. Sci. Instrum.*. **84**, 123105, 2013.

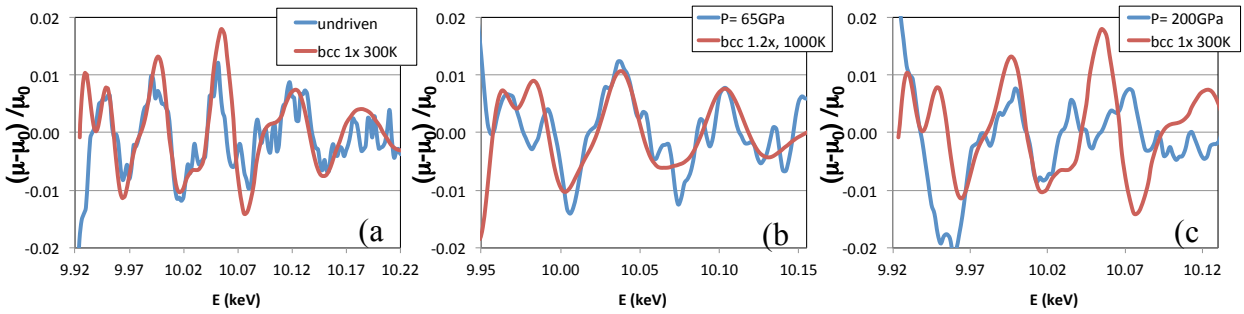

Figure 1: *EXAFS data of Ta (a) at ambient conditions; (b) at 65 GPa; and (c) at 200 GPa. The measurements are shown in blue and the calculated EXAFS spectra for the bcc phase are shown for comparison in red. The 200 GPa demonstrate that Ta is no longer in the bcc phase at such high pressures.*

III. Hydrodynamics

A. Mix Width Measurements of Accelerated Copper Foam on OMEGA (PI: K. Baker)

This campaign evaluated two experimental configurations for determining the mix width of accelerated copper foams, and measured the effect of the internal structure of the copper foams on the measured mix width so as to compare the experimental results with simulations. All the targets were cylindrical shock tubes with a reduced-density copper (Cu) foam, 1 g/cc, pusher accelerated into a low density carbonized resorcinol formaldehyde (CRF) foam at 50 mg/cc. The Cu foams, which could contain voids as large as 5 to 10 um, were characterized via x-ray computed tomography at either the Advance Photon Source or with an X-Radia MicroXCT. An example is displayed in Figure 1. In the first configuration, the copper foam was reduced to an 800 μm diameter cylinder for the 120 μm closest to the Cu/CRF interface (to reduce edge effects in the images) and radiographed using the EP backlighter. The removed Cu foam was replaced with CH. The second experimental configuration used a nickel He-α backlighter at 7.66 keV and a modified target design to accommodate the lower energy and also minimize edge effects. Figure 2 shows a radiograph of the accelerated copper foam obtained using the EP backlighter in the first configuration, and Figure 3 shows a lineout through the radiograph. The mix width for this foam was determined to be 135 um.

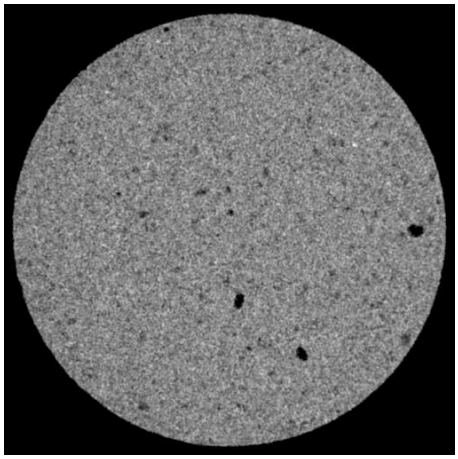

Figure 1: *Reconstructed density profile of a copper foam. The voxel size of the reconstructed density is cube ~7 um per side.*

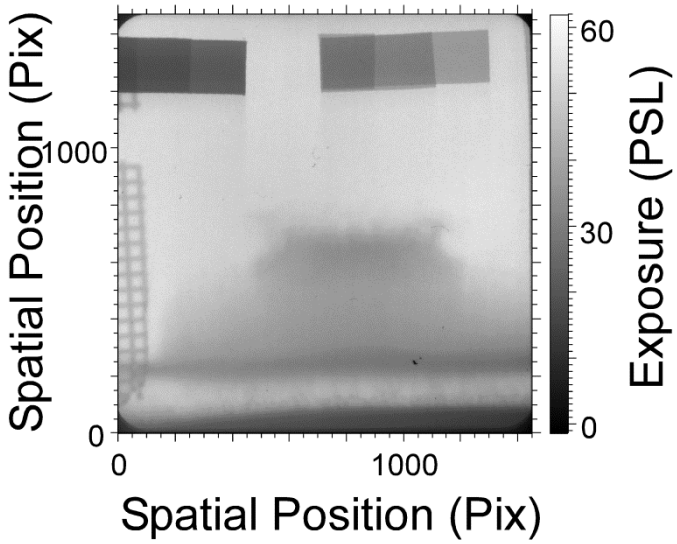

Figure 2: *Radiograph of an accelerated copper foam 25 ns after the start of the hohlraum drive.*

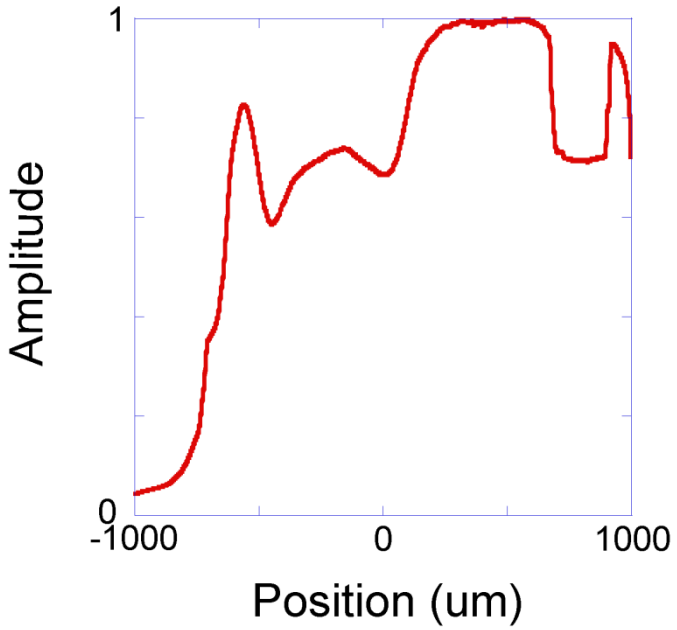

Figure 3: *Vertical lineout through the accelerated copper foam shown in Fig. 2.The mix width comes from the 10% to 90% region between 0 and 250 um of the graph.*

B. Shock Transit Time Measurements on Novel CH Foams (PI: K. Baker)

Shock breakout times from X-ray driven samples of newly formulated $CH_{1.6}$ foams were measured on this campaign, for comparison with traditional carbonized resorcinol formaldehyde (CRF) foams. The foams were positioned as packages on the end of a gold halfraum. To account for differences in the drive between experiments, the hohlraum drive history was measured via breakout from an aluminum witness plate, and also via shock speeds in α-quartz using VISAR. As illustrated in Figure 1, all shots returned good VISAR data, showing the breakout times of the foam into and out of the VISAR window, and the breakout of the shock from the $CH_{1.6}$ or CRF foams. The corresponding VISAR unfold of the drive is inset in the lower right hand corner of the figure. Comparison of experimental breakout times with simulations showed very good agreement with the CRF foams, and good agreement with the $CH_{1.6}$ foams.

Additionally in this experiment, three Ross pair channels were implemented in DANTE to look at the gold M-band emission from the laser-driven hohlraum: Saran, silver and Mo. Four Ross pair channels were also implemented in a time-integrated X-ray pinhole camera to look at the M-band wall emission: Si, Zr, Mo, Saran and Kapton. These also look promising for determining the time-integrated M-band spatial and spectral distribution on the wall.

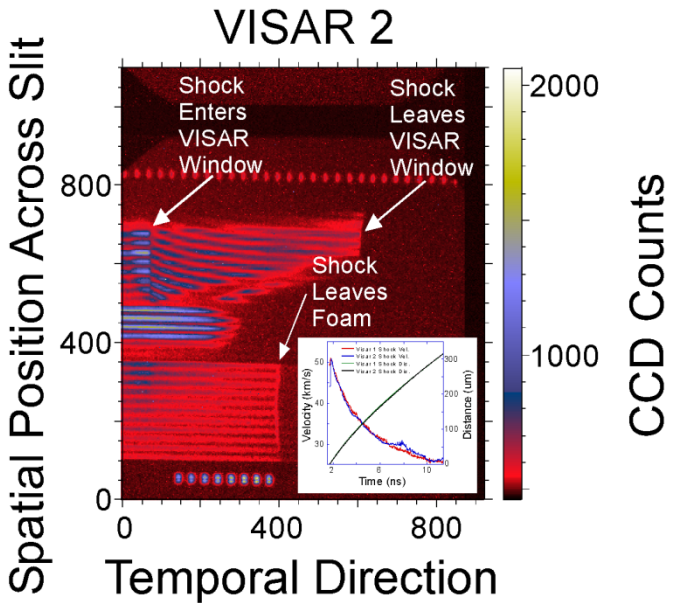

Figure 1: *Drive and sample shock speed measurements for $CH_{1.6}$ foams.*

C. Copper Foam Shock Breakout Measurements on OMEGA (PI: A. Moore)

High-Z metal foams made via a copper ceramic casting process and with approx. $1/10^{th}$ solid density (~1 g/cc) have been developed at LLNL and are being produced routinely at AWE. This campaign investigated the relative shock propagation in foams having 1.0 μm characteristic pore sizes, to qualify the equation of state for use in future experiments. Propagation of a single shock through a material sample is an established technique to quantitatively validate the EoS model for that material via the simple dependence of the shock velocity on the pressure and so internal energy of the material, but it had not been applied previously to these novel foams. The platform to measure the shock transit-time in Cu foams was unchanged from prior campaigns of this type, using a 1.6 mm diameter, 1.0 mm long hohlraum driven by 5.5kJ of 351nm laser energy using 15 beams of the OMEGA Laser System. But to improve the measured accuracy of the x-ray drive from the hohlraum, an Al witness sample was added, so that the target package on the halfraums included a foam sample with a polystyrene ablator along-side a 60μm aluminum sample backed by 300μm quartz. When the shock breaks out into the quartz, it can be measured directly using the active shock break-out (ASBO or VISAR) diagnostic, and the pressure history at the hohlraum ablator interface can be inferred.[1]

In the experiments the drive pulse shape was varied to extend the density and temperature regimes probed. A 1.0ns square pulse shape was used on experiments with the C_8H_8 ablator, and a 2.7ns ramp-shaped laser pulse was used on experiments without this ablator. The copper foam samples were 0.7 mm in diameter and nominally 0.35 mm in thickness, with a nominal density of 1.0 g/cc. On these experiments the hohlraums reached a peak effective radiation temperature of 208±5eV.

Data from the streaked optical pyrometer (SOP) was obtained on five shots, an example of which is shown in Figure 1(c). These data indicate that some spatial structure exists in the shock travelling through the Cu foam, but the average shock break-out time was still determined to within ±3%. The ASBO was used on three shots to measure the decaying shock velocity as a function time in the quartz, returning data very close to pre-shot predictions.

References:

1. J. Edwards *et al.*, *Phys. Rev. Lett.* **92**, 075002. (2004)

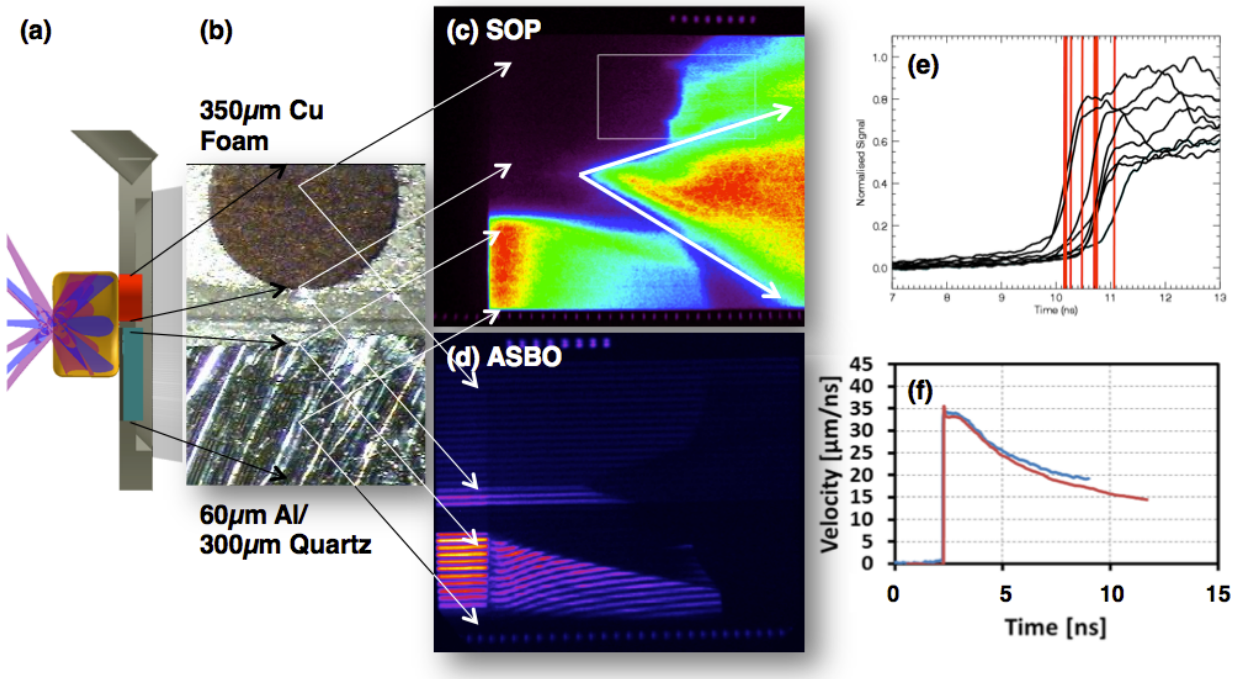

Figure 1: *Streaked Optical Pyrometer (SOP) and active shock break-out (ASBO) data from shot 71664 – Hohlraum with no CH ablator drive by SS2704vA01. (a) VisRad diagram of the target. (b) Images of the Cu foam (355μm thick at density 1.084 g/cc) and Al/Quartz surface viewed by the ASBO & SOP. (c) Raw SOP image data with arrows highlighting edge effects due to the expanding joint between the Cu foam and Al/quartz samples. (d) Raw ASBO image data showing shock breakout times. (e) Normalized optical emission due to shock break-out showing that the shock in the Cu foam arrived at 10.48 ± 0.33ns, (f) Shock velocity in the quartz peaked at 34 km/s, and was within 3km/s of preshot predictions.*

D. High energy point projection backlighter experiments on OMEGA (PI: K. Baker)

The goal of this campaign was to evaluate high-energy backlighters for use on the NIF. The backlighter energies needed on NIF range from 35 to 45 keV. Previous conversion efficiency (CE) measurements with short pulse lasers at 1ω indicated a CE of $7x10^{-5}$ for tin through $4x10^{-5}$ for Samarium. These efficiencies are close to meeting NIF required fluences using the Advanced Radiographic Capability short-pulse laser being deployed on NIF, but would require the NIF detector to be placed much closer to the target than previously. However, the previous experiments had been conducted with wire backlighters, and other laser-target geometries are possible to improve x-ray fluence yields. In this campaign, the Omega 3w lasers were used to drive a point projection backlighter with a Ta pinhole to reduce the source size. Tin and Samarium targets were fielded, with and without a prepulse, and using either thick solid or exploding foil plasmas. Figure 1 illustrates the target geometry. The Transmission Crystal Spectrometer (TCS) measured the tin and samarium spectra. Figure 2 shows the TCS spectra from these shots, together with a prior 1ω short pulse silver wire backlighter spectrum.

The highest conversion efficiency was seen for thick foils without prepulse. The pre-pulsed plasmas may have refracted the drive laser beams, leading to a reduction of yield. Resolution tests using a sharp opaque gold edge had blurry features for all the targets, indicating a large source size. This could be improved with a significantly thicker or more advanced pinhole substrate.

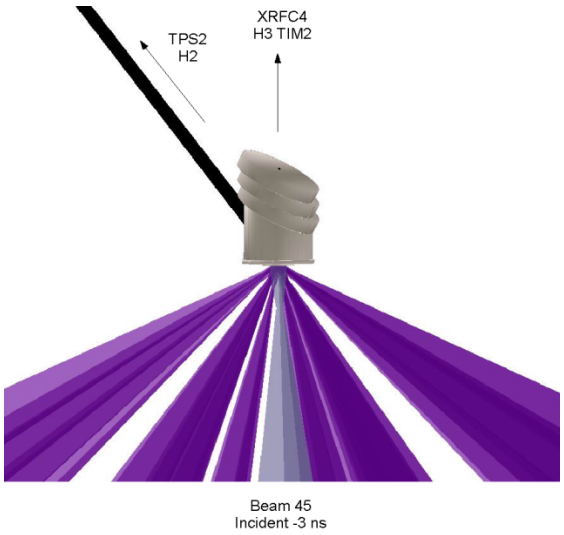

Figure 1: *Target geometry used to evaluate the efficacy of high energy point-projection backlighters. The pinhole substrate was 200 um thick Ta, sandwiched between 100 um disks of CH to limit the number of hot electrons reaching the pinhole substrate*

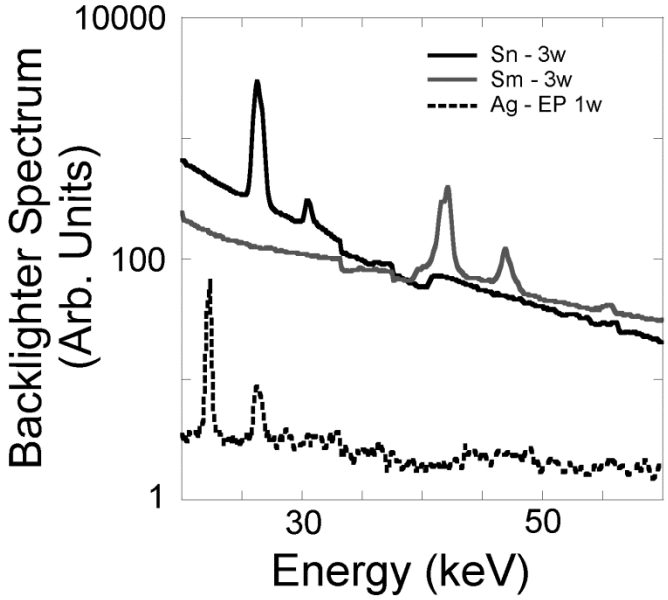

Figure 2: *Backlighter spectra measured with the TCS.*

E. Radiographic Techniques for Drive Symmetry (PI: D. Martinez)

Hohlraum experiments were performed on the OMEGA laser system to develop and exploit radiographic techniques to study the symmetry of foam balls illuminated with hohlraum x-rays. Using a joint OMEGA-EP configuration, 10 μm thick Ag wire backlighters mounted on 300x300 μm square, 10 μm thick polyimide foils were irradiated with the ~1 kJ short-pulse EP beam in a configuration similar to that expected on the NIF Advanced Radiographic Capability short-pulse laser, with a pulse duration of ~50 ps at a laser intensity of ~$2x10^{17}$ W/cm^2. Point-projection X-ray radiographs of the targets with a magnification of ~40 were measured on image plates using the HERIE diagnostic positioned ~50 cm from target chamber center. The high-energy bremsstrahlung spectrum was used to diagnose the target. Figure 1 shows data from resolution test objects illustrating the radiographic signal and contrast, which were consistent with previous Ag μ-wire experiments using Omega EP and demonstrated 17 μm resolution. Transmission of the backlighter through a Cu step wedge was measured and used to infer the hot electron temperature by modeling the backlighter with a simple single temperature bremsstrahlung spectrum. These experiments produced high-quality radiographs and established a baseline for future Complex Hydrodynamics experiments on National Ignition Facility (NIF).

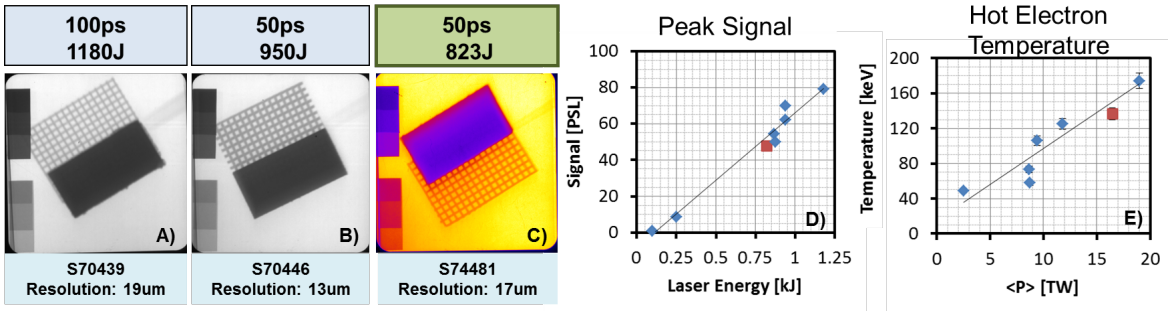

Figure 1: *Silver μ-Wire Backlighter from past Toto experiments (A & B) compared with current performance (C). Trends in the peak signal and approximated hot electron temperature show results are consistent with previous Ag μ-wire experiments using the same filtering and diagnostic.*

F. Proton Heating of Copper Foams on OMEGA EP (PI: A. Moore)

High-Z metal foams made via a copper ceramic casting process at approximately 10% of solid density (~1 g/cc) provide a novel target material for use in high-energy density physics experiments on NIF, Orion and OMEGA. However, for experimental results to be constraining to radiation hydrodynamics simulation codes, the materials need to be well characterized, with a good understanding of the material opacity and equation of state (EoS). These proton-heating experiments developed a platform to access the equation of state of the Cu Foam via isochoric heating of the material with protons, and investigated the feasibility of scaling the approach to NIF using the upcoming Advanced Radographic Capability short-pulse laser.

Proton heating offers a novel way to measure the low temperature equation of state, since the energy is absorbed near-isochorically by the Cu foam, especially when compared to heating with x-rays or via direct laser irradiation.[1] If the density profile of the expanding plasma is measured, then the isentrope can be extracted directly. These experiments studied density measurements of proton-heated discs of Al and Cu foam, and Cu wires. The proton source consisted of a 10μm thick, 500μm diameter Au foil irradiated by a high-intensity (~$1x10^{18}$ W/cm^2), 1053nm, 10ps laser pulse from the OMEGA EP laser. This generated a proton beam through target-normal sheath acceleration (TNSA).[2] The Cu foam and other samples were placed 2.0mm from the proton source along the normal to the Au disc. To radiograph the sample expansion, a Ni foil backlighter was positioned 5mm from the sample perpendicular to the foam disc normal. Beamlines 1, 3 and 4 delivered 1.0ns, 351nm laser pulses to this Ni foil with a 10ns delay after the short-pulse beam, generating He-α x-rays (7.9keV) to radiograph the expanding Cu foam.

The proton spectrum was measured using a radiochromic film (RCF) stack 25mm past the Au disc source. Figure 1 shows the proton 'auto-radiograph' measured using the RCF stack when the Cu foam disc was present and heated by the protons. Figure 2 shows the success of the area-backlit radiography in obtaining images of the unheated and heated Cu foams. Work is ongoing to establish the relative contribution of x-ray and proton heating at the front surface of the Cu foam.

References:

1. P. K. Patel, *et al.*, *Phys. Rev. Lett.* **91**, 125004 (2003)
2. S. C. Wilks *et al.*, *Phys. Plasmas* **8**, 542 (2001)

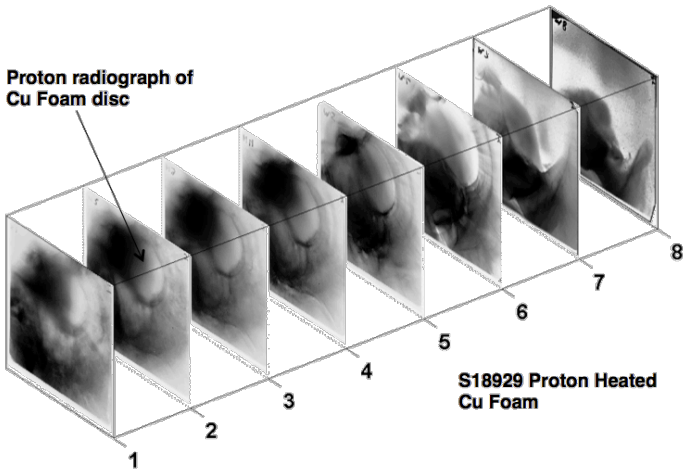

Figure 1: *'Proton auto-radiograph' of the proton heated Cu foam, measured by a radiochromic film pack in the neat –target arm diagnostic.*

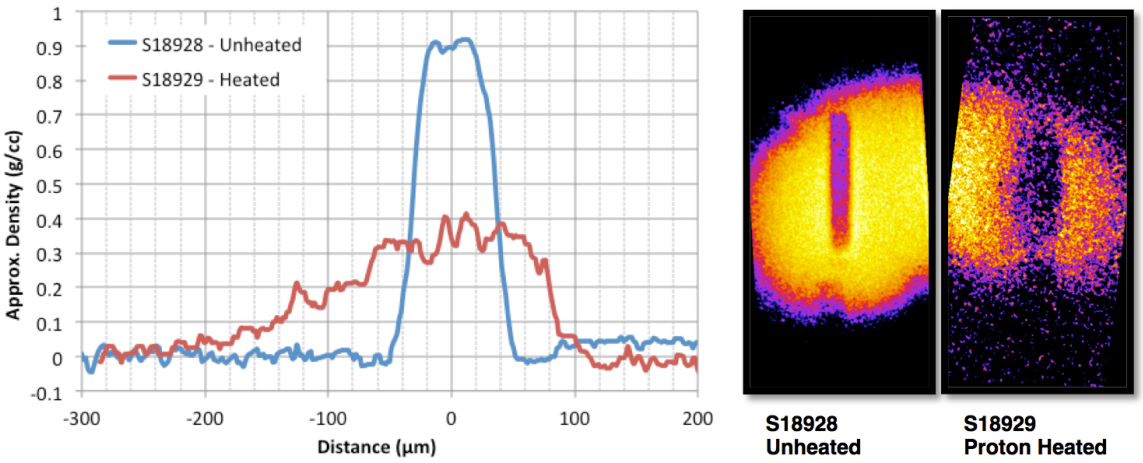

Figure 2*: Radiograph of unheated (S18928) and proton-heated (S18929) Cu foam after 10.0ns of free expansion. The density profile of the heated foam is obtained assuming no significant changes to the opacity of the Cu foam when heated, and calibrating the backlighter x-ray spectrum using the predicted transmission of the 0.9g/cc unheated foam.*

IV. Radiation Transport and Opacity

A. X-ray Spectroscopy of Fully Characterized Non-LTE Gold Plasmas (PI: G. Brown)

with J.A. Emig, M.E. Foord, R.F. Heeter, D. Liedahl, C.A. Mauche, J. S. Ross, M.B. Schneider, K. Widmann (LLNL) and in collaboration with D. Froula and J. Katz (LLE).

Experiments at the National Ignition Facility have shown a need for a more precise understanding of the radiative properties of non-LTE gold, to improve X-ray drive simulations of laser-driven hohlraums used in inertial confinement fusion and other areas of high-energy-density physics. Expanding upon prior work,[1] the AuNLTE-14A campaign fielded laser-heated beryllium-tamped gold-iron-vanadium foils, with the following primary objectives: (1) high-resolution measurements of time-resolved gold M-band spectra from 2 to 5.5 keV, simultaneously with (2) measurements of the plasma electron temperature (T_e) via K-shell emission from helium-like V and Fe ions, (3) independent measurements of T_e using Thomson scattering in a transmission geometry, and (4) measurements of the sample density by time-resolved spectral imaging of its expansion normalized to the initial thickness.

The campaign acquired data for three different target types: (a) "thicker" and (b) "thinner" mixtures of Au, Fe and V, and (c) a mixture of Fe and V without Au. Simultaneous K-shell spectra from He-like Fe^{24+} and V^{21+} and M-band Au, together with expansion images, were acquired for all three types of target. After some adjustments, ion acoustic wave "transmission" Thomson scattering data were successfully obtained, for the first time, from plasmas at electron densities > $10^{21}/cm^3$. Some of the IAW data were obtained simultaneously with the other measurements, with measured T_e in the ~1 keV range. Although detailed data analysis is ongoing, this suite of measurements is potentially the most comprehensive non-LTE data set recorded to date. If confirmed in the final analysis, this will yield improved validation benchmarks for non-LTE models.

1. R.F. Heeter *et al.*, *Phys. Rev. Lett.* **99**, 195001 (2007).

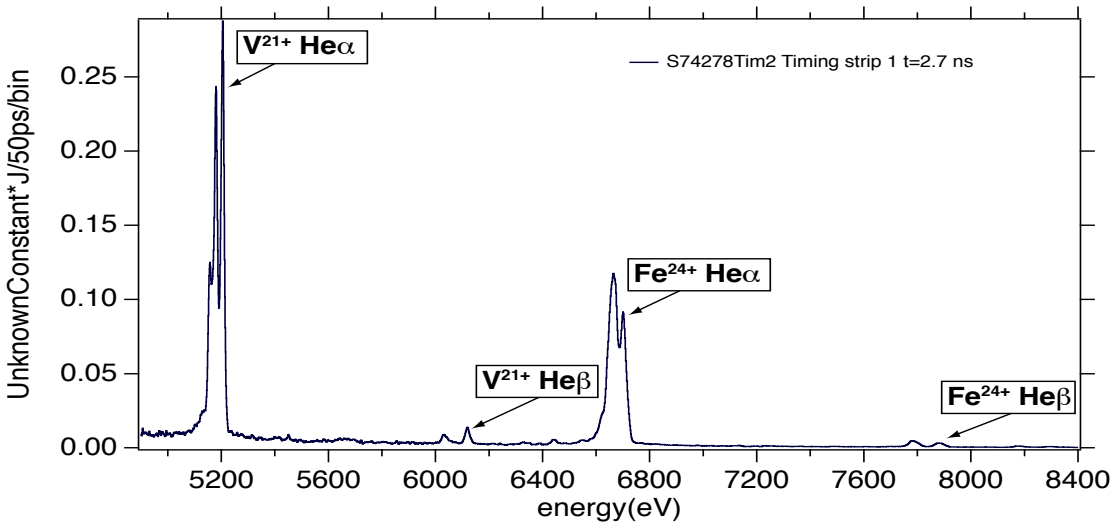

Figure 1: *Spectrum measured by the MSpec spectrometer of the X-ray emission from K-shell transitions in highly charged vanadium and iron.*

V. Material Dynamics and Strength

A. Classical Rayleigh-Taylor Growth (PI: C. Huntington)

Within the Material Strength effort aimed at assessing the strength of various metals at high pressure and high strain rate, the goal of the Classical Rayleigh-Taylor campaign is to measure Rayleigh-Taylor (RT) growth of samples that behave "classically," i.e. can be fully modeled using a fluid description. Without the stabilization of strength, classical RT growth is characterized by a growth rate $\gamma = \sqrt{kgA_n}$, where k is the wavelength of the unstable mode, g is the acceleration, and the Atwood number A_n quantifies the magnitude of the density jump at the interface. Acceleration of the sample in the experiment is provided by the stagnation of a releasing shocked plastic "reservoir," which is directly driven by approximately 1 kJ of laser energy. The growth of pre-imposed ripples is recorded using transmission x-ray radiography of a vanadium He-α source, where the opacity of the sample is calibrated to the ripple amplitude. The FY14 campaigns collected data for ripples with 30 μm, 60 μm, and 120 μm wavelengths. An example of 60 μm data is shown in Figure 1. The area backlighter generates an image with varying brightness across the image; analysis is performed on the brightest region, and a background curve that captures the shape of the x-ray illumination is subtracted. The pre-shot metrology and measured ρr of the driven sample together yield the growth factor, which is compared to models of RT growth.

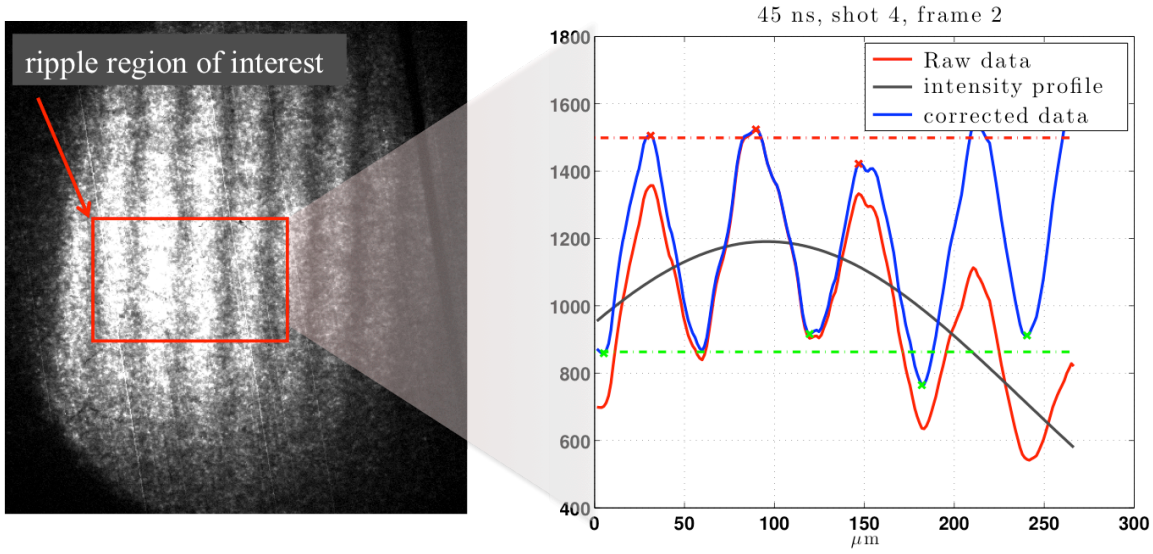

Figure 1. *A region of interest is selected from a piece of data, shown in red on the left. The integrated profile of these ripples is shown on the right in red, and the "corrected" trace is shown in blue, after being adjusted by the gray curve.*

VI. X-Ray Source Development and Application

A. Calibration of the NIF X-Ray Spectrometer (PI: S. Regan, LLNL/LLE Collaboration)

With F. Pérez, M.A. Barrios Garcia, K.B. Fournier, G.E. Kemp, J. Pino, J. Emig, and S. Ayers (LLNL); M. Bedzyk, M.J. Shoup, A. Agliata, B. Yaakobi, and F.J. Marshall (LLE) and J.Jaquez, M. Farrell and A. Nikroo (GA)

The NIF X-ray Spectrometer (NXS) is an elliptically bent crystal spectrometer providing both time-resolved and time-integrated spectral measurements. The NXS covers a spectral range from 2-18 keV in ten discrete spectral windows each corresponding to a particular crystal configuration. Two FY14 Omega campaigns provided data for a photometric calibration for all 30 NXS crystals (each configuration has three interchangeable crystals), by uniformly irradiating millimeter-scale spherical targets coated with various cocktails of mid-Z elements. The targets were designed to generate either L-shell or K-shell emission within the energy range of the NXS' spectral windows. Five different targets were designed for these calibration shots, using Cr-Ni-Zn, Zn-Zr, Si-Ag-Mo, and Ti-Cr-Ag coatings, and an uncoated CH target used to measure continuum emission. Target emission was recorded by five different spectrometers for each shot: 3 NXS's and two XRS spectrometers. The XRS spectrometer crystals were absolutely calibrated off-line, and provide absolute x-ray yield from which the photometric calibration of the NXS crystals will be derived. All data was recorded onto Fuji SR-type image plates which are also being calibrated off-line, in order to provide an end-to-end absolute calibration for the NXS spectrometer.

In preparation for the Omega calibration shots, hydrodynamic simulations using HYDRA and ARES were performed to predict the emission from the metal-coated targets. Figure 1 compares these simulation results with the absolute x-ray yields measured by the XRS spectrometer for all four metal-coated targets. Here target types A, B, C, and D correspond to Si-Mo-Ag, Ti-Cr-Ag, Cr-Ni-Zn, and Zn-Zr coatings, respectively. The predicted line emission agrees qualitatively with the XRS results. Details on the simulations and comparison with the XRS data have been published.[1] A more rigorous comparison between model and measured data will be performed once the absolute NXS calibration is finalized. Figure 2 shows sample data measured for one of the NXS spectrometers. This shot used a Cr-Ni-Zn coated target; measured data on the top and bottom image plate are shown on the left, with corresponding lineouts on the right. Several K-shell emission lines from Cr, Ni, and Zn were observed and identified.

1. F. Pérez, *et al.*, "The NIF x-ray spectrometer calibration campaign at Omega," *Rev. Sci. Instrum.* **85,** 11D613 (2014)

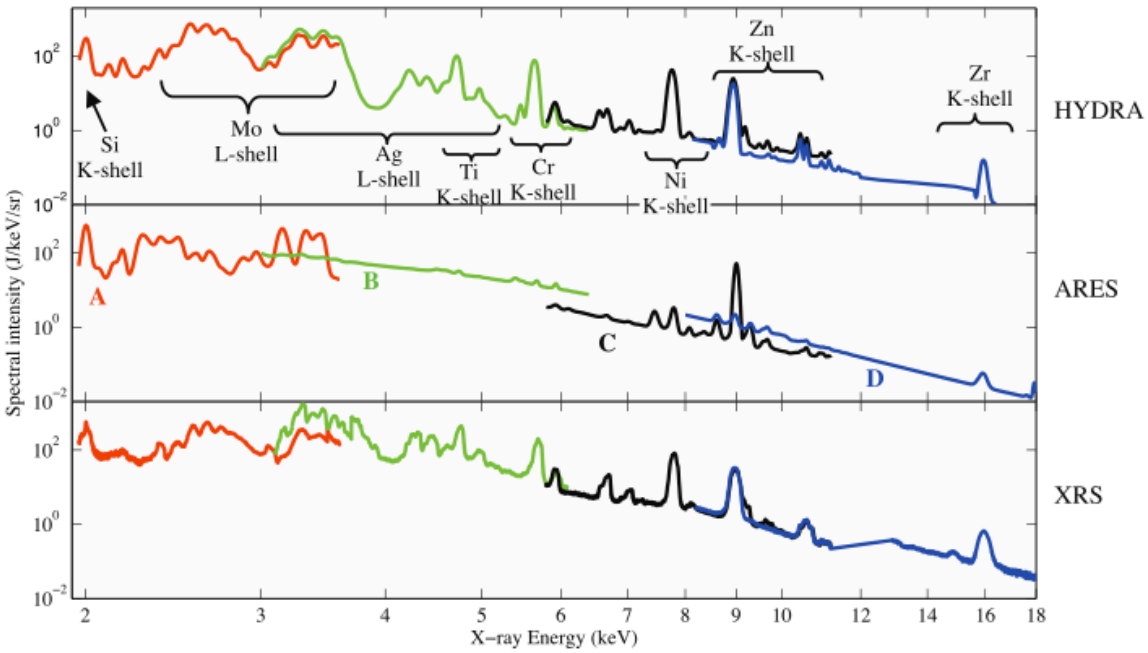

Figure 1: *Simulated spectra using HYDRA and ARES hydrodynamics codes is compared to measured XRS data for metal coated targets A (SiMoAg), B (TiCrAg), C (CrNiZn), and D (ZnZr). Good qualitative agreement between data and simulations is observed.*

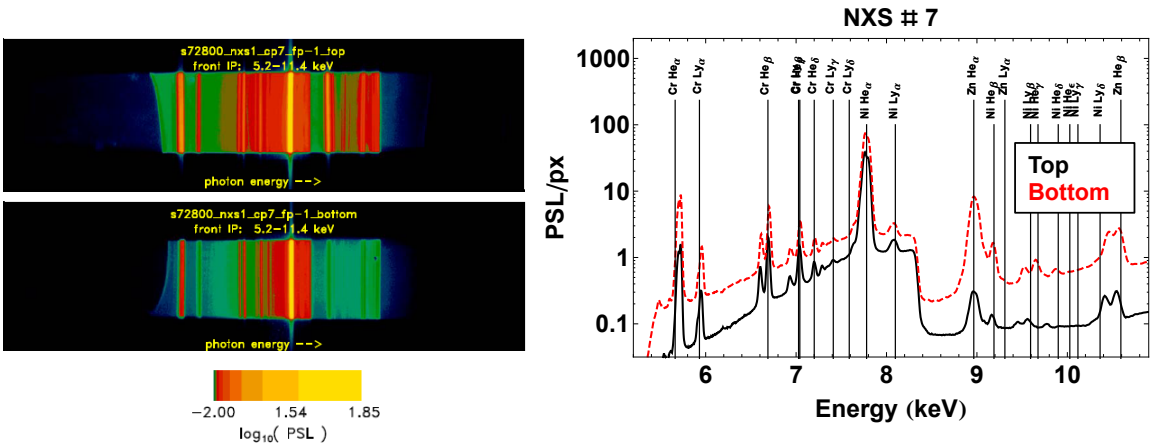

Figure 2: *Measured data on NXS for one of ten configurations. Measured spectra recoded onto an SR image plate are shown on the left, with corresponding data lineouts on the right.*

B. X-ray Source Fluence Measured as a Function of Viewing Angle (PI: M. Barrios Garcia)

With M.J. May, K.B. Fournier, F. Pérez, and J.D. Colving (LLNL); F. Girard and B. Villette (CEA); S. Seiler and J. Davis (DTRA); and J. Fisher and C.D. Newlander (Fith Gait Technologies)

The NSView campaign was designed to understand target fluence as a function of viewing angle for x-ray source applications, to better understand the fluence delivered to material samples and other test objects using these or similar targets as X-ray sources. In this campaign, stainless-steel-lined cavities were symmetrically driven with ~20 kJ of 3ω light delivered in 1 ns. To provide distinct view angles for the diagnostics fielded, three different laser-target orientations were used throughout the day. The target X-ray emission was recorded with a suite of x-ray diagnostics, enabling characterization of both the temporal evolution and spectral content of the source.

Figure 1 shows the measured spectra recorded using the Dante and DMX spectrometers, for view angles relative to the target symmetry axis of 0°, 42°, and 79°, and 5°, 46°, and 75°, respectively. These instruments observe a pronounced view angle dependence on the measured flux for x-ray energies below 4 keV, but little to no dependence on view angle for the Fe K-shell emission at higher energies. The observed x-ray emission from 4-9 keV, describing the Fe K-shell, is consistent with a volumetric emitter that is optically thin, and thus independent of view angle. The emission from 2-4 keV is also consistent with a volumetric emitter, once geometric and optical-depth corrections are considered. These factors cause the x-ray yield to decrease as a function of increasing view angle. For x-ray emission between 0-2 keV, corresponding to the Fe L-shell, the observed yields peak at angles ~42°-46°, and show the largest variation between view angles. This low energy x-ray yield is also the dominant contribution to the total x-ray production. A spectral reconstruction model developed to match these observations suggests the x-ray output between 0-2 keV is best described as a surface emitter, where the emission originates from the cavity inner walls and LEH. Figure 2 compares this model with the data. Future work will measure x-ray emission for intermediate angles to better constrain the model, and investigate other types of targets.

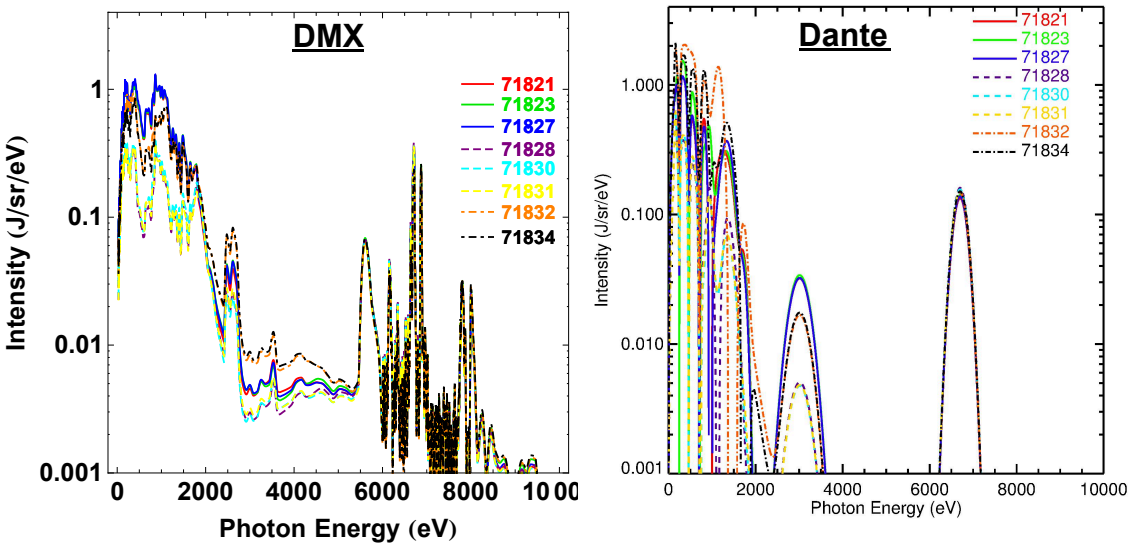

Figure 3: *Measured DMX (left) and Dante (right) time integrated spectra.*

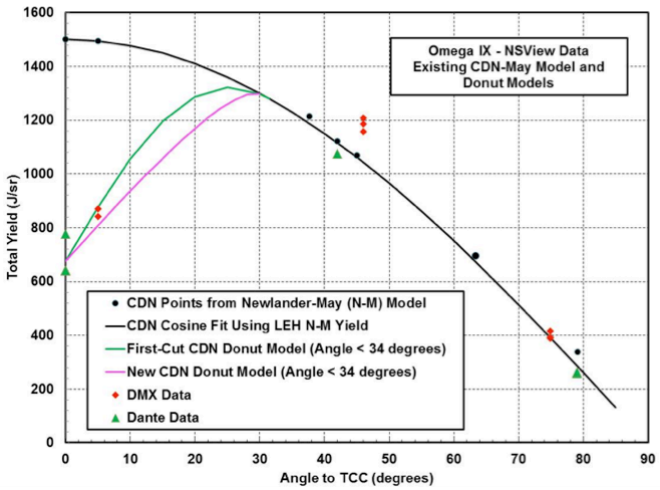

Figure 4: *Dante and DMX total x-ray yield as a function of view angle, compared to developed model.*

C. Optimizing X-ray Emission from Nanostructured Copper-Doped Foams (PI: F. Pérez) with J.D. Colvin, K.B. Fournier, M.J. May, S.O. Kucheyev and S. Charnvanichborikarn (LLNL); and T. E. Felter (Sandia)

In FY13 the X-Ray Source Development team, funded by the Defense Threat Reduction Agency, started to study the x-ray emission from laser-irradiated Cu-doped foams. The goal is to generate bright, ns-class x-ray pulses with ~9 keV photon energies. A novel fabrication technique successfully produced Cu-doped carbon foams with densities below 50 mg/cm^3 for FY13 shots. In 2014 this effort continued, developing another novel foam fabrication method and yielding, for the first time, doped foam densities below 10 mg/cm^3.

These C/Cu foams (Figure 1a) were irradiated by 40 beams of the Omega laser to generate x-rays (Figure1b). Various foams, with densities ranging from 5 to 50 mg/cm^3, were shot on two campaigns. Measurements of the x-ray yield show that the optimal density is close to 10 mg/cm^3, where the conversion efficiency from laser energy into Cu K-shell x-ray energy reaches 0.8%. The dynamics of the laser-foam interaction were also investigated using framing and streak cameras, revealing that the low-density foams are heated over a much larger volume (Fig. 1c). X-ray spectra also provided information on the plasma temperature. These measurements are currently being used as simulation benchmark, with the wide range of densities providing tight constraints.

This research has also led, in FY14, to pure-Cu foams under 20 mg/cm^3, which will be fielded in FY15 experiments. This type of material has never been fabricated before, and is expected to achieve even higher x-ray yield.

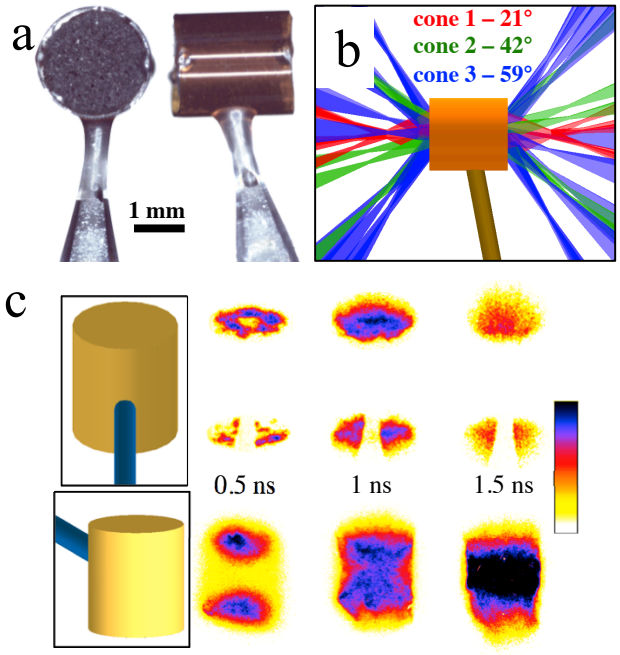

Figure 1: *(a) Foam sample held in a plastic tube. (b) Laser irradiation pattern of the Omega laser. (c) X-ray emission images at different times relative to the beginning of the irradiation. The top and bottom rows correspond to foams of 50 and 8 mg/cm^3 density, respectively.*

Laboratory Basic Science Experiments

1. Ablative Richtmyer-Meshkov Experiments (PI: D. Martinez)

The ablative Richtmyer-Meshkov (RM) instability driven from laser imprinting in the presence of a phase inversion was explored on the Omega-60 laser system. Figure 1 shows the experimental configuration. Planar 30 and 50-μm thick CH targets were directly driven with three UV beams using a 3 ns square pulse shape, total energy of ~0.7 kJ, and laser intensity of ~ $5x10^{13}$ W/cm^2. Initial target modulations were imposed by laser imprinting, using a beam with a special 2D phase plate with a modulation wavelength of ~30 microns and timing advanced by ~200 ps relative to the other drive beams, which had regular Omega distributed phase plates (DPP's). Growth of target modulations was measured with gated x-ray radiography using samarium (~1.8 keV), and tantalum (~2.2 keV) backlighters, 10 μm spatial resolution and 80 ps temporal resolution. The backlighters were driven with a 2 ns square pulse shape at ~ $3x10^{14}$ W/cm^2 using seven additional UV beams. Figure 2(a) shows a typical radiograph of the RM instability for a shot using laser imprinting. For comparison, foils with preimposed modulations were also used, to observe the differences between the RM instability from preimposed modulations, and the data are shown in Figure 2(b). Although the modulations were not purely orthogonal, the power spectrum shows the modulations are sufficiently separated Figure 2(c). Figure 3 shows that the imprinted and preimposed modulations follow the same growth trajectory, suggesting that imprint, in the observed case, had little to no influence on the RM instability after the initial seed. Simulations using the CHIC code from CEA and the DRACO code from LLE disagree with the trajectory of the modulations; one possible explanation is the codes are over predicting the ablation velocity. Investigation into the disagreement is ongoing.

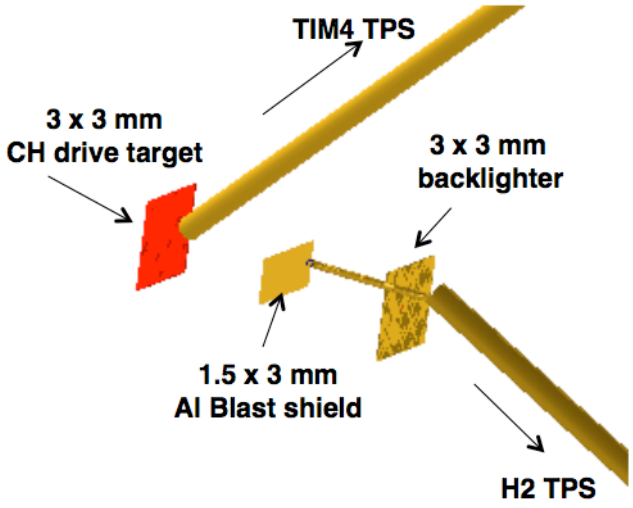

Figure 1: Experimental configuration for FY14 ablative Richtmeyer-Meshkov experiments.

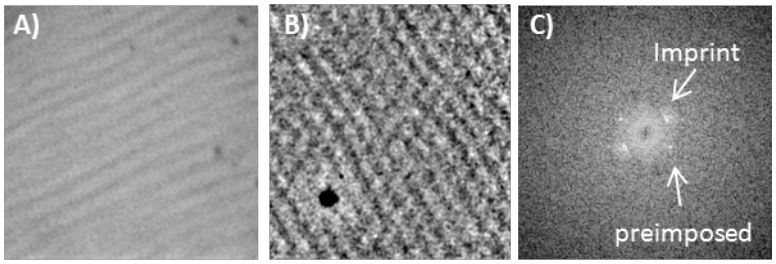

Figure 2: *Data showing a) imprint modulations in 30µm thick foil at 0.8ns, b) imprint and preimposed growth at 0.8ns in CH 50µm thick target and c) the Fourier power spectrum of b).*

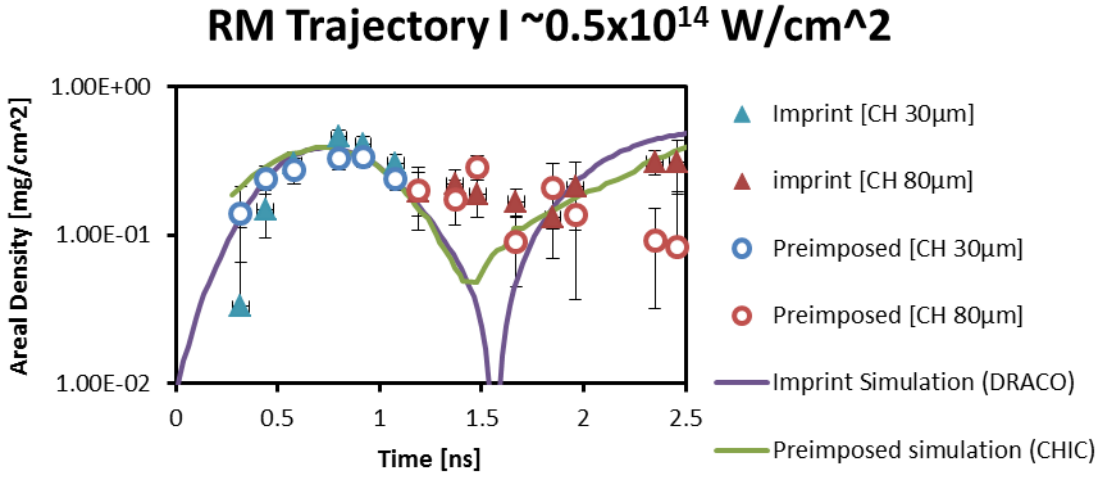

Figure 3: *Richtmyer-Meshkov growth for 30µm and 80µm thick CH foils for imprinted (triangles) and preimposed (open circles) modulations. Shock breakout is expected at 0.9ns for 30µm and 2.4ns for 80µm thick foils.*

2. Astrophysical Collisionless Shock Experiments with Lasers (ACSEL) on EP
(LBS PI: H.-S. Park; Shot PI: Channing Huntington)

The ACSEL collaboration is studying high velocity plasma flow interactions and the role of self-generated or amplified magnetic fields in such systems. Study of these phenomena is essential to understanding a range of astrophysical systems, including gamma-ray bursts, supernova remnants, and young stellar objects. The FY14 experiments using Omega-EP expanded on the collisionless shock platform common to ACSEL (LBS) and MagShock (NLUF), with the former concentrating exclusively on plasmas without externally applied magnetic fields. Irradiating a pair of opposing planar targets with 2.2 kJ (EP), counter-propagating flows are created, each with bulk velocity near 1000 km/s. The flows interact near the midplane between the targets, where the interpenetrating plasma is susceptible to a range of instabilities, including the two-stream and Weibel instabilities.

The FY14 campaigns studied on the effect of varying the target material, including the effect of collisional flow from higher Z target materials. Figure 1 shows comparison data obtained for CH_2 (the same as most of previous studies), Al, and Cu targets. The central magnetic field advection feature[1,2] is very different between these target types. The data shows that the two horizontal features, thought to be associated with piled up magnetic fields from the Biermann battery at the laser spot, move apart over time, which is different from collisionless flow experiments where the two features stay at the same place. This is likely due to pressure buildup in the interaction region, which pushes the features apart. Both FLASH and Osiris simulations show qualitative agreement with the experimental data. On the other hand, the actual size of the interaction region remains narrow, and the fact that the two plates are still horizontal indicates that probably the turbulence is not very developed. This implies that turbulence in the collisional flow plays an important role in the formation of the magnetic field. Further experiments are planned in FY15.

References:
1. N. L. Kugland, D. D. Ryutov, *et al.* Self-organized electromagnetic field structures in laser-produced counter-streaming plasmas. *Nature Physics* **8**(11):809–812, 2012.
2. N. L. Kugland *et al.*, "Visualizing electromagnetic fields in laser-produced counter-streaming plasma experiments for collisionless shock laboratory astrophysics", *Phys. Plasmas* **20**, 056313 (2013).

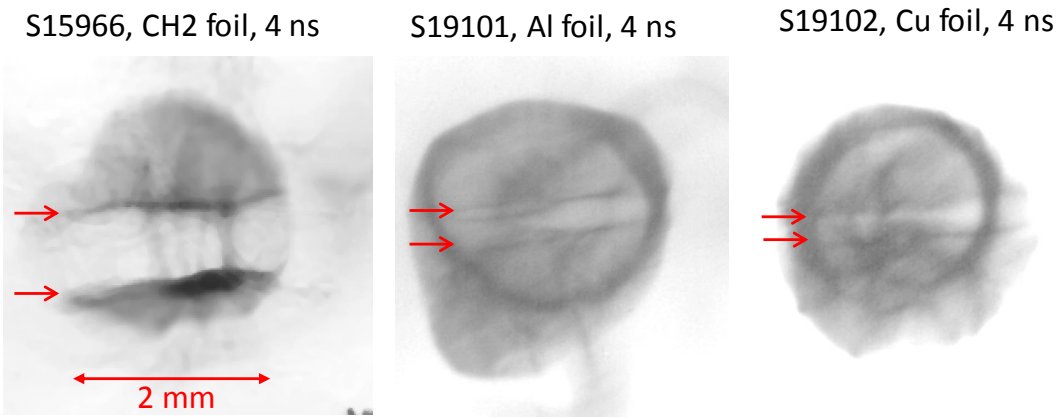

Figure 1: *Comparison of magnetic fields from interpenetrating high velocity flows. The higher Z targets create colliding flows that affect the magnetic field advection generated by the Biermann battery from the target surface. This indicates that turbulence in the collisional flows play an important role in the formation of the magnetic field.*

3. Creation and Measurement of Novel High-Pressure Electride States of Matter (PI: T. Ma)
with A. Pak, B. Bachmann, S. Le Pape, T. Doeppner (LLNL)

Density functional theory (DFT) simulations predict a new material phase in highly compressed matter, where valence electrons, instead of becoming delocalized, actually bunch up in interstitial pockets. This creates an electron lattice co-existing within the ion lattice. This experiment used x-ray Thomson scattering to search for the existence of this electride phase by probing the lattice spacing that corresponds to the electrides.

Magnesium foils, 100 μm thick, were shock compressed to 5-8 Mbar using a single-sided ramp drive utilizing 9 Omega beams with up to 800 J total. The shocked samples were probed using Zn He-α x-rays (8.9 keV) at a time corresponding to peak pressure. By varying the scattering angle between the shots, the static structure factor was directly probed, where the scattering profile would show pronounced peaks at low k values due to the additional reflections and interferences of the electride lattice. Excellent scattering data was acquired at the various phases of Mg reached under varying shock conditions, however, preliminary data analysis does not seem to show scattering variations that would immediately indicate the existence of electrides. Further data analysis is required.

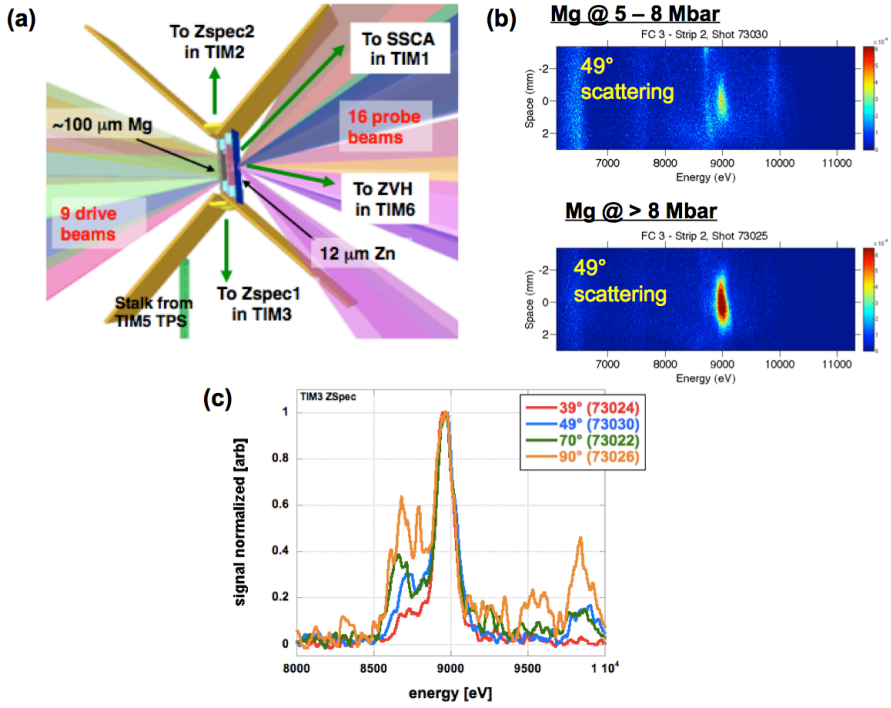

Figure 1: *(a) Experimental configuration, (b) Raw scattering data taken at 49° for Mg compressed to between 5-8 Mbar (FCC phase) and > 8 Mbar (SH phase), and (c) Comparison of scattering profiles for four shots taken at various scattering angles for Mg shock compressed to FCC (5-8 Mbar) phase.*

4. Fast Ignition Using Elliptical-Tip Cone-in-Shell Targets

LBS PI: P. Patel (LLNL); **Shot PI:** F. Pérez (LLNL)**; Co-investigators:** H. Sawada (UNR); W. Theobald and A. Solodov (LLE); L. C. Jarrott and F. N. Beg (UCSD); M. S. Wei (GA); A. Link, Y. Ping, and H. S. McLean (LLNL)

The Fast-Ignition (FI) approach to inertial fusion has potential to achieve higher energy gain compared to central hot spot ignition schemes. Fast Ignition uses a separate short-pulse ignition laser to locally heat the fuel core near the time of peak compression. This ignition laser is focused inside the tip of a re-entrant gold cone and accelerates a large number of high-energy electrons. The efficiency of heating the fuel to thermo-nuclear conditions can be greatly increased if the electrons accelerated from the laser interaction region can be guided to the dense fuel.

This year's experiments investigated electron beam guiding using resistivity discontinuities through structured material interfaces. The Omega-EP picosecond laser was focused on a slab of plastic containing short aluminum wires of various shapes. Laser-generated electrons tend to stay localized inside the wire, due to magnetic fields generated along the resistivity discontinuity. As illustrated in Figure 1, a copper slab was attached at the back of the CH-Al foil to detect the location of the electrons exiting the foil. Wires of three formats were used: traversing the whole slab ("long"), traversing only a short portion of the slab ("short"), or in the shape of an ellipsoid. The latter have been predicted to provide better focusing characteristics, in the manner of elliptical mirrors in optics. The electrons passing through the Cu foil induce Cu-Kα x-ray emission, which was imaged using the spherical crystal imager as shown in Figure 2. The presence of the wires clearly produced structure in the electron beam, showing that some guiding is occurring. However, in this experiment, the ellipsoids were not proven to be more efficient than straight wires. A simulation effort is benchmarking the current models to these results, and extending the models to ignition-scale situations. It is expected that the guiding effects will be enhanced in full-scale scenarios.

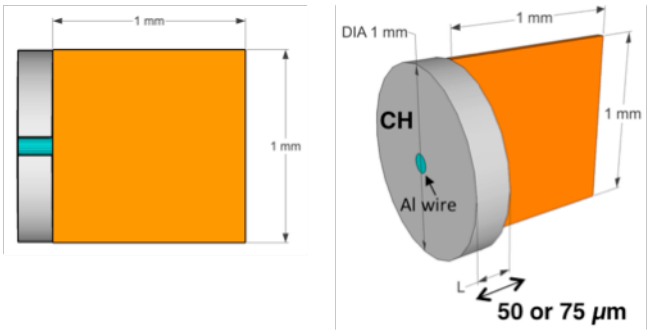

Figure 1: *Schematic of the targets.*

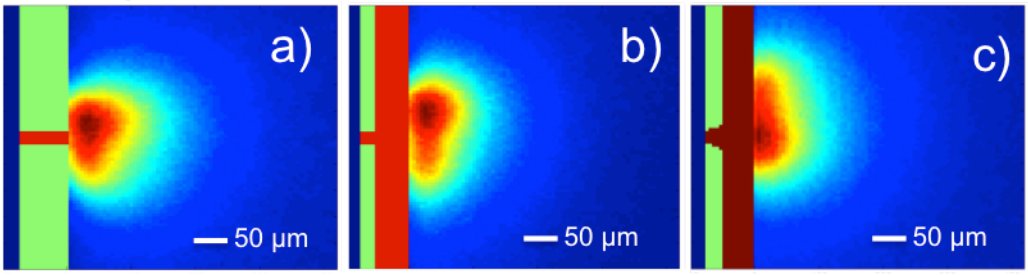

Figure 2: *Cu-Kα images, reflecting the shape of the electron beam through the Cu foil. The green blocks correspond to plastic, and the red blocks correspond to Al. The long wire is a), short wire is b), and the ellipsoid structure is c).*

5. Initial Applications of the Sustained-Drive "Gatling-Gun" X-Ray Source (LBS PI: R. Heeter; Shot PI: D. Martinez)
with J. Kane (LLNL), R. Mancini (UNR), B. Villette and A. Casner (CEA)

This FY14 campaign on Omega-EP continued the successful development of "Gatling-Gun" multi-hohlraum-array x-ray sources in FY13, in which a radiation temperature of 90eV was produced for 30ns. This capability is important for multiple physics experiments, including investigations of (a) x-ray photoionization equilibrium at relatively low plasma densities ~10^{18} ions/cm^3, and (b) the hydrodynamics of pillar formation from directional radiation relevant to the Eagle nebula.

The FY14 campaign used a copper three-hohlraum array, shown in Figure 1A, to drive simultaneously a Ti photoionization sample and a hydrodynamics sample, demonstrating the capabilities of the Gatling gun hohlraum. The three hohlraums were heated in succession using three UV beams, each with 10ns square pulses and 3.8kJ of energy. The hohlraum temperature was measured with CEA's Mini-DMX, which again recorded 80-100eV over 30ns.

The photoionization sample consisted of a 0.6mm x 0.6mm x 0.5μm Ti foil sandwiched between two 1μm thick tamper layers of 1mm x 1mm CH. The emission spectrum, recorded using the VSG diffraction grating spectrometer, showed strong Cu emission from the hohlraum and a weak signal in the expected range of the Ti L-shell emission lines. Interpretation of the spectrum is ongoing.

The hydrodynamics sample consisted of 50 mg/cc resorcinol formaldehyde (R/F) foam with an embedded, solid density CH ball of 350μm diameter. The hydrodynamics of the sample was studied using a Ti area backlighter driven by a 1ns, 1.25kJ UV beam with a 500μm focal spot. The backlit image was imaged onto a single-frame x-ray framing camera with a 4x4 20μm pinhole array, providing a detailed composite radiograph from the multiple images. Figure 1 shows the recorded images, in which the shock front has propagated into the R/F foam past the CH ball.

Both aspects of the experiments successfully demonstrated the application of the Gatling gun, resulting in additional shots for further, specific applications.

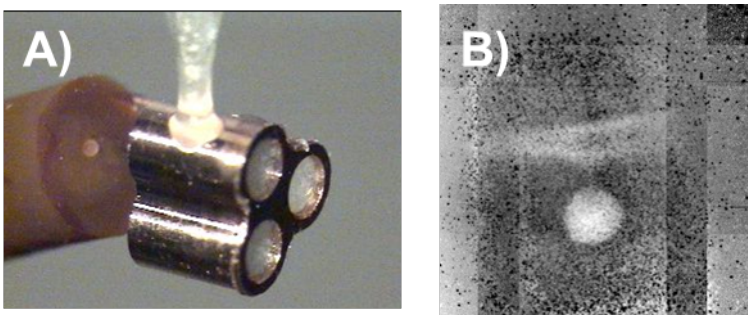

Figure 1: *A) Target image showing the Gatling gun triple hohlraum and attached R/F foam with embedded solid density CH ball. B) Radiograph reconstructed from a 16-pinhole array gated at T = 35ns.*

6. Search for Nuclear Excitation by Electron Capture in Osmium and Thulium (LBS PI: L. Bernstein; Shot PI: R. Heeter)

with D. Bleuel, J. Emig and S. Ross (LLNL) and M. Comet, V. Meot, F. Phillippe and C. Reverdin (CEA)

Nuclear excitation by electron capture is an exotic process which has never been observed in the laboratory, but in stellar plasmas it is thought to populate low-lying nuclear excited states and may modify neutron capture and other astrophysical rates. In laser-driven plasmas created on ~1 ns timescales, NEEC may be observed through gamma decays re-emitted on ~5 ns timescales, after the plasma has cooled and x-ray emission is negligible. Earlier experiments searched for 8.41 keV NEEC in ^{169}Tm hohlraums (made from rolled thulium foil), using erbium as a null comparison, and found an ambiguous signature.

The FY14 experiments revisited these measurements and also searched for 9.76 keV NEEC decay emission in isotopically pure Os-187 lined Ti hohlraums, with Os-192 as a null comparison. Ti was chosen because it could be electroplated with Os-187, while not providing any x-ray contamination in the NEEC spectral band. The hohlraums were 0.6 mm in diameter and were driven at 10kJ in 1 ns using 20 beams of Omega-60.

In the experiments, optical Thomson Scattering data obtained 300 μm outside the cavity laser entrance hole showed electron temperatures of ~4.3 keV and densities ~4×10^{20}/cm^3. A suite of time-integrated and time-resolved X-ray spectra were obtained with CEA's XCCS, and LLNL's MSPEC and HENWAY spectrometers; the XCCS view is illustrated in Figure 1. These measurements failed to show NEEC emission in either ^{169}Tm or ^{187}Os within the sensitivities of these instruments, but are able to set an upper bound on the highly uncertain NEEC rates. Improved measurements with larger quantities of ^{187}Os and more sensitive spectrometers could further constrain NEEC rates.

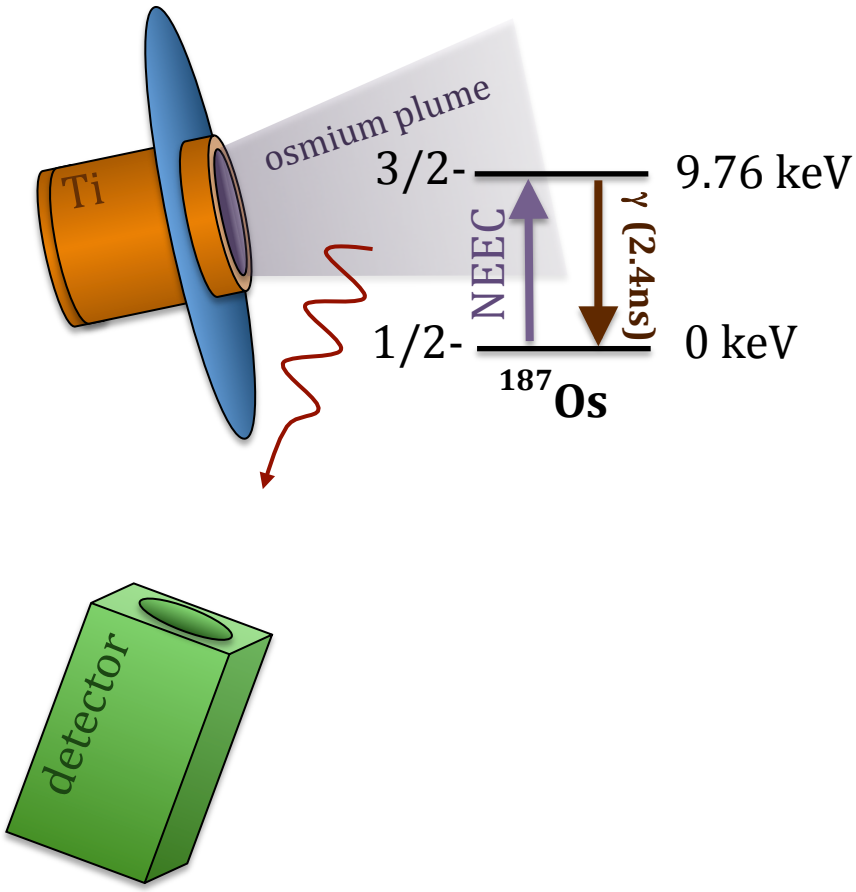

Figure 1: *Experimental Configuration showing the Os-lined Ti hohlraum with over-the-shoulder view of the CEA XCCS spectrometer, together with the level diagram for NEEC and subsequent gamma decay in Osmium-187.*

7. Exploring Pair Plasmas and Their Applications (PI: H. Chen)

The FY14 pair plasma experiments on Omega-EP used the short pulse beams to produce jets of electron-positron antimatter pairs, and focused on measuring the pair yield and its dependence on the target material. The experiments successfully probed the basic physics processes involved in pair generation, and the data reveal discrepancies between experiments and theory. By alternating beams and streamlining diagnostic operations, a total of 31 shots were performed in just 2 shot days.

The EP short pulse beams (~1 kJ in 10 ps) irradiated targets of 1 mm thick Sn, Ta, Au, Pb and U. Unexpectedly high positron yields were recorded from the Ta, Pb and U targets (see preliminary results in Figure 1), in disagreement with the expected ~Z^4 scaling from the Bethe-Heitler process. The reasons for the discrepancy, once understood, should significantly impact future pair production experiments. Previous experiments used gold targets almost exclusively. They showed that quasi-monoenergetic relativistic positron jets are formed during high-intensity irradiation of thick gold targets [1, 2], and that these jets can be strongly collimated [3] using the magnetized-inertial fusion electrical delivery system (MIFEDS) [4]. The external field produces a 40-fold increase in the peak positron and electron signal [3]. The FY14 results suggest that the pair density could be increased up to an order of magnitude with U instead of Au targets. This would enable the laboratory study of relativistic pair plasmas that are important to understanding some of the most exotic and energetic systems in the universe [5].

References:

[1] H. Chen *et al.*, *Phys. Rev. Lett.* **102**, 105001 (2009).
[2] H. Chen *et al.*, *Phys. Rev. Lett.* **105**, 015003 (2010).
[3] H. Chen *et al.*, *Phys. Plasmas* **21**, 040703 (2014).
[4] O. Gotchev *et al.*, *Rev. Sci. Instrum.* **80**, 043504 (2009).
[5] H. Chen *et al.*, *High Energy Density Physics* **7**, 225 (2011).

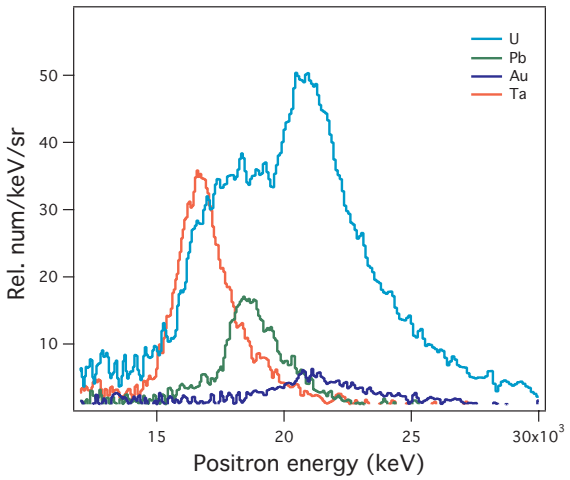

Figure 1: *The Z-dependent positron yield measurement on OMEGA EP in FY2014.*

8. Structure and Equation of State of Solid and Superionic Warm Dense Water

LBS PI: J.R. Rygg (LLNL); **Shot PIs:** F. Coppari and M. Millot (LLNL)

The structure and equation of state of solid and superionic warm-dense water at Uranus' and Neptune's core conditions were investigated, to explore a proposed superionic phase; essentially a solid lattice of oxygen ions surrounded by fluid-like diffusing protons. Its existence in the deep interiors of icy giant planets would have a dramatic impact on their internal structure and evolution.

The experiments on Omega-60 employed new laser dynamic compression techniques, novel liquid-cell targets, and advanced diagnostics, including both optical diagnostics and x-ray diffraction. Multishock compression in these experiments squeezed initially liquid water into solid and superionic ices at pressures of several megabar, while keeping the temperature below 0.5 eV. Data were obtained using streaked optical reflectivity, pyrometry and interferometric Doppler velocimetry (VISAR), as well as x-ray diffraction. Ongoing analysis of the recently obtained x-ray diffraction data will provide unprecedented insight on the equation of state and structure of solid and superionic megabar water ices in the portion of phase space shown in Figure 1.

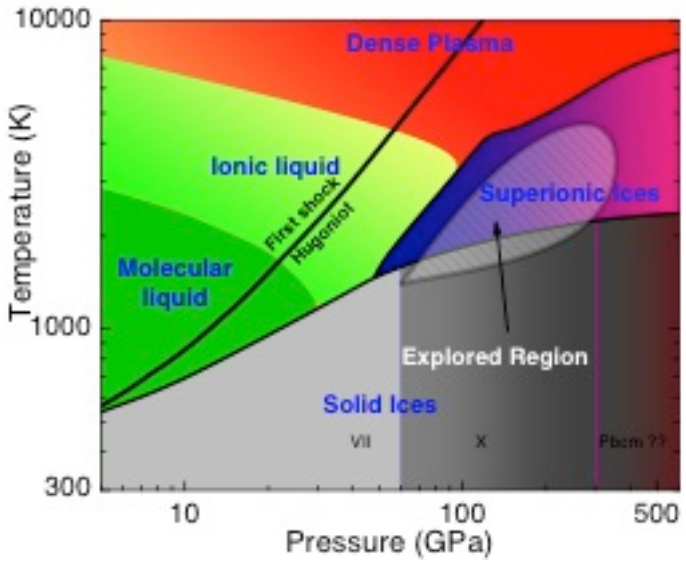

Figure 1: *Pressure-Temperature phase diagram of warm dense water, showing the region explored with multishock compression of liquid water using ultrafast optical diagnostics and x-ray diffraction on the Omega Laser system.*

9. Thermonuclear Reactions in Stellar Plasmas

LBS PI: D. McNabb (LLNL); **Shot PI:** M Gatu Johnson (MIT)

Two distinct LBS "stellar rates" campaigns were fielded in FY14, in conjunction with a related NLUF effort and with extensive collaboration between LLNL, MIT, LLE and LANL. The main goals of the first campaign were to study stratification (between T and ^{3}He) and nuclear product spectra in T^{3}He implosions (with trace D in the fuel). Understanding the impact of stratification on implosion yields is a key step towards using the implosion platforms developed in inertial confinement fusion (ICF) research to measure cross sections relevant to stellar and big bang nucleosynthesis. T^{3}He(D) is an ideal fuel mixture to study stratification, because of the many measurable nuclear yields produced from these implosions (T^{3}He-p, T^{3}He-d, D^{3}He-p, DT-n, TT-n). Trace quantities of D are not expected to significantly impact stratification between the T and ^{3}He majority ions. Although detailed data analysis and post-shot simulations are in progress, Figure 1 shows preliminary measured D^{3}He/DT yield ratios (points with error bars) for these shots as a function of partial ^{3}He pressure in the fuel. Three different fill mixtures were shot, in order to test a theoretical prediction that stratification effects will cancel out in T^{3}He fuel at 90:10 T:^{3}He.[1] Also shown in the figure is the pre-shot simulation of the D^{3}He/DT ratio, from hydro simulations (ARES) not considering possible stratification effects. Stratification between T and ^{3}He would show up as a deviation from the predicted ratio. Pending post-shot simulations, the preliminary indication is that stratification effects are small in these experiments.

In the second experiment the γ rays from the p+D fusion reaction were measured for the first time in an ICF plasma, at a center of mass (Gamow peak) energy of ~16 keV. This reaction is relevant to astrophysics. In particular, during big-bang nucleosynthesis it produces ^{3}He (at particle energies >~100 keV), and in protostars and brown dwarfs it is the primary source of nuclear energy (at particle energies <1 keV). The low energy of this γ (5.5 MeV) necessitated use of the new GCD-3 detector by LANL. Excellent data was acquired for the p+D reaction, highlighted in Figure 2. These shots also measured the DD-γ for the first time in ICF, which is the primary source of background for the p+D measurement.

[1] G. Kagan and X.Z. Tang, *Physics Letters A* **378**, 1531 (2014).

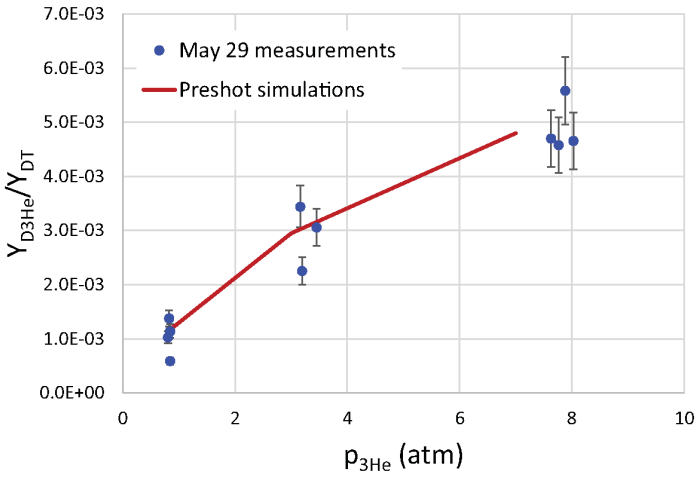

Figure 1: *Preliminary measured D^{3}He-to-DT yield ratios as a function of partial ^{3}He fill pressure in the capsule (points with error bars). Also shown is the ratio predicted in preshot simulations (red line) assuming no stratification of the T and ^{3}He.*

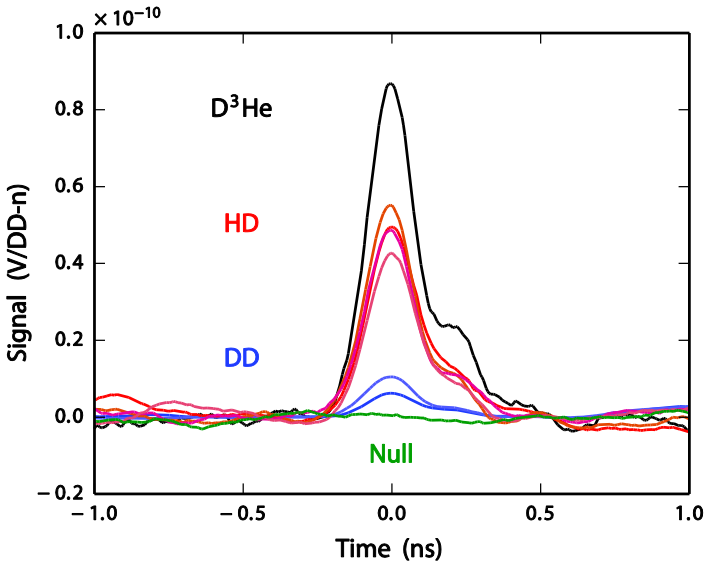

Figure 2: *Cherenkov detector signals for the p+D experiments, showing 4 shot types: D^3He (detector calibration, black), HD (primary signal, red), DD (background, blue), and Null (background, green). Excellent p+D fusion data was acquired for the first time.*

10. Charged Particle Stopping Power Measurements on Omega-EP (PI: S. Nagel, LLNL)
with A. Zylstra (MIT)

Calculations of charged-particle energy loss in ICF-relevant plasma conditions still depend on untested theories. To address the need to validate these theories, a platform is being developed on Omega-EP to measure charged-particle energy loss. Strongly coupled or fully degenerate conditions are difficult to obtain, but warm dense matter (WDM) plasmas that have temperatures of several tens of eV and approximately solid densities (10^{22}-10^{23}) are well within the moderately coupled and degenerate regimes.

The experimental schematic is shown in Figure 1. A short-pulse beam is used to generate energetic protons via the target normal sheath acceleration (TNSA) mechanism to probe a warm foam target. The foam target is x-ray heated using a halfraum driven by three long pulse UV beams. Compared to previous campaigns on EP, this method showed an improvement of the proton beam smoothness, better pointing of the proton beam through the material, and reduced crosstalk between the heating and proton probing. This therefore significantly advanced the platform, and new measurements are planned.

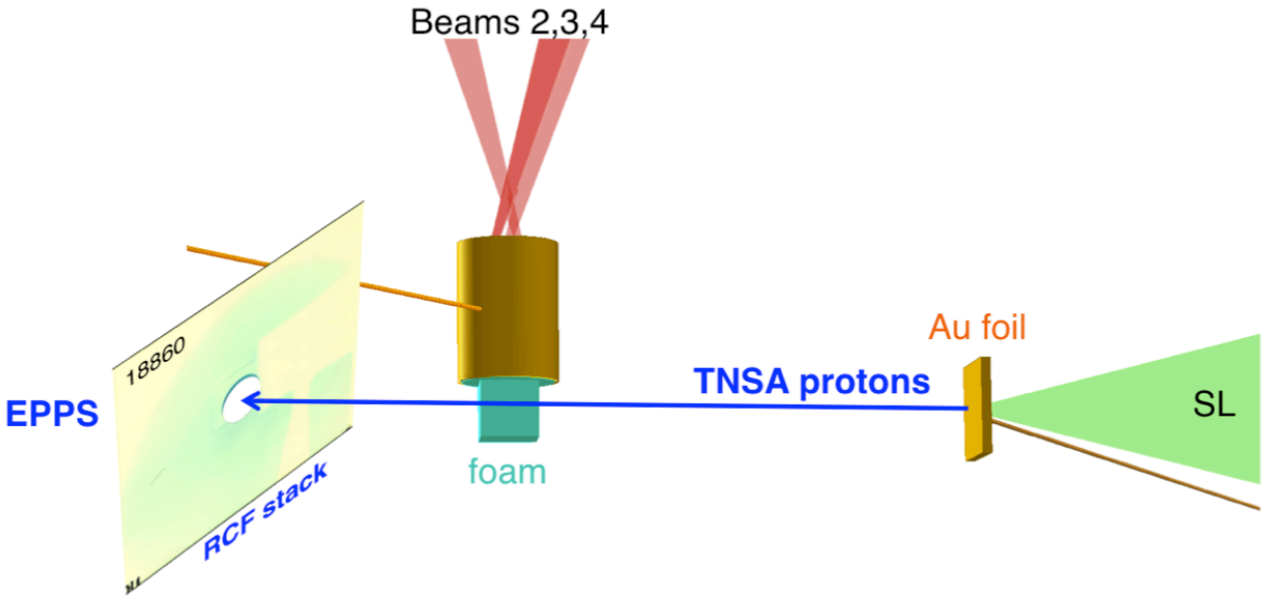

Figure X: *Experimental schematic. One OMEGA EP short-pulse laser beam is used to create the probing protons, whose proton beam profile and spectra were characterized by a new combination of both radiochromic film and the electron-proton-positron spectrometer EPPS. The other three beams are used to heat the foam target.*

11. Viscosity Measurements on Liquid Silica (PI: P.M. Celliers)

with M.A. Barrios and A.E. Gleason

This was the third of a series of campaigns to demonstrate a method for determining the viscosity of a high pressure fluid created by the propagation of a strong shock front through an initially transparent sample. The measurement technique is based on observing the evolution of a spectrum of perturbations imposed on a multi-Mbar shock front passing through the sample material. The viscosity of the liquid state just behind the shock front is expected to influence the decay rate of the perturbations as the shock front propagates, and detailed measurements of the perturbation state can be compared with calculations in order to assess the viscosity. The sample under study is liquid silica (SiO_2), produced by propagating the shock through samples of either alpha-quartz or fused silica. The viscosity of high pressure liquid silica has obvious geophysical relevance, and measurements in the Mbar domain are not possible with conventional methods. Two earlier campaigns in 2010 and 2012 examined the shock response to perturbation spectra that were generated by both random and coherent patterns imposed on the sample surface at the interface with the ablator. These initial experiments demonstrated the feasibility of using the OMEGA High Resolution Velocimeter (OHRV) to produce quantitative measurements of the multi-mode velocity perturbations directly from the surface of the reflecting rippled shock front.

In the 2014 experiments, the shocks were driven using a hohlraum coupled to a 50 μm CH (PMMA) ablator followed by the sample. Although measurements on water samples as well as silica were envisaged for this campaign, that option assumed successful fabrication of novel water cell targets, which turned out to be more difficult than expected and precluded collecting a data set on water in this campaign. Nevertheless, excellent data was obtained for silica.

In the experiments, as the shock passed through this interface the perturbations were transferred to the shock front, which were detected and measured quantitatively by the OHRV. Figure 1 shows an example velocity spectrum for a ~200 GPa shock driven into fused silica. The spectrum shows the presence of nodal zones – modes whose instantaneous oscillation velocity was near zero at the time of the OHRV probe. These nodal patterns are expected from the multi-mode solution of the rippled shock evolution. Details of the amplitudes and positions of the nodes depend on the viscosity. Model calculations employing an analytical expression derived by Miller & Ahrens[1] are used to estimate the mode amplitude as a function of spatial frequency, shown in Figure 2. Here, we see that the observed spectrum is consistent with viscosities near 2 Pa-s (20 poise).

1. G.H. Miller and T.J. Ahrens, *Rev. Mod. Phys.* **63** 919 (1991), equation 127.

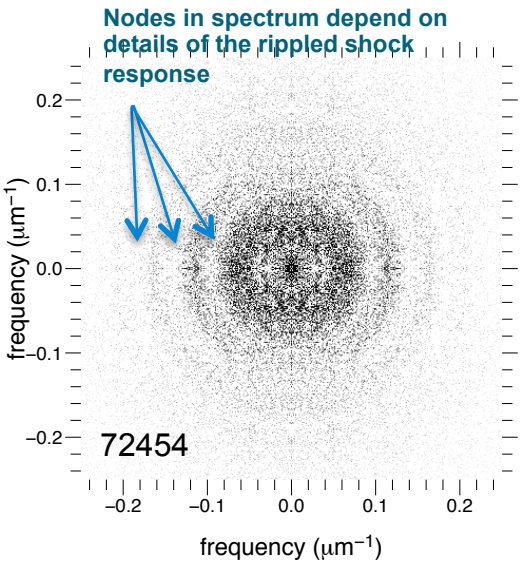

Figure 1: *Two-dimensional velocity spectral density of a rippled shock front generated at a roughened interface between a PMMA ablator and a fused silica sample recorded 800 ps after passage of the shock through the interface (shot 72454). Gray scale is proportional to mode velocity amplitude. Nodal regions are where the mode velocity is near zero at the time of the probing, corresponding to those modes which are undergoing a velocity reversal at the probing time.*

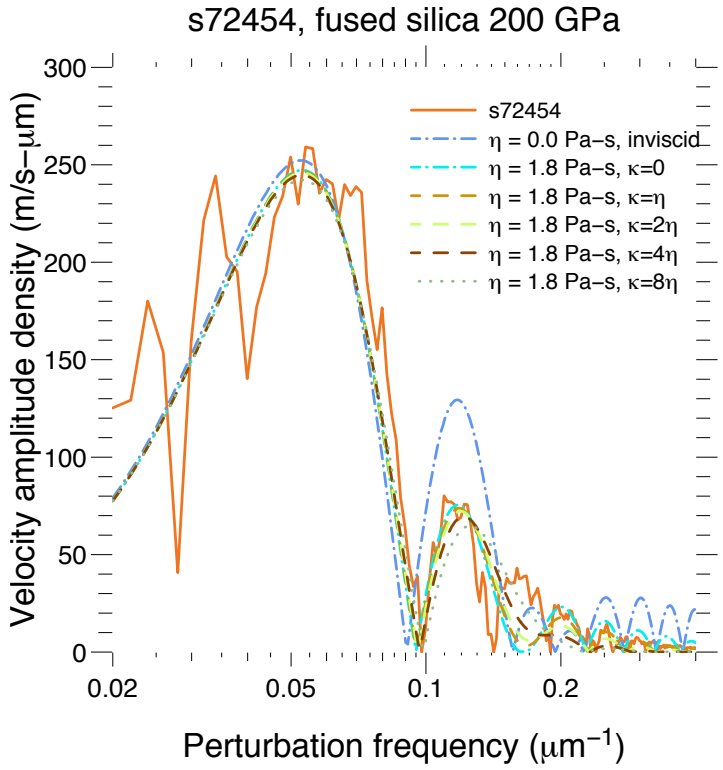

Figure 2: *Background subtracted and azimuthally averaged mode amplitude as a function of mode spatial frequency. The first node is near 0.09 μm^{-1}, the second near 0.14 μm^{-1} and so on. Also shown are theoretical mode amplitudes expected for the inviscid response and several viscous cases, where the bulk viscosity κ is taken to be different multiples of the shear viscosity, η. The data suggest the viscosity is near 1.8 Pa-s (18 poise).*